

Transregional transport of haze particles from the North China Plain to Yangtze River Delta during winter

Zhang, Jian; Yuan, Qi; Liu, Lei; Wang, Yuanyuan; Zhang, Yinxiao; Xu, Liang; Pang, Yuner; Zhu, Yanhong; Niu, Hongya; Shao, Longyi; Yang, Shushen; Liu, Hang; Pan, Xiaole; Shi, Zongbo; Hu, Min; Fu, Pingqing; Li, Weijun

DOI:

[10.1029/2020JD033778](https://doi.org/10.1029/2020JD033778)

License:

None: All rights reserved

Document Version

Publisher's PDF, also known as Version of record

Citation for published version (Harvard):

Zhang, J, Yuan, Q, Liu, L, Wang, Y, Zhang, Y, Xu, L, Pang, Y, Zhu, Y, Niu, H, Shao, L, Yang, S, Liu, H, Pan, X, Shi, Z, Hu, M, Fu, P & Li, W 2021, 'Transregional transport of haze particles from the North China Plain to Yangtze River Delta during winter', *Journal of Geophysical Research: Atmospheres*, vol. 126, no. 8, e2020JD033778. <https://doi.org/10.1029/2020JD033778>

[Link to publication on Research at Birmingham portal](#)

Publisher Rights Statement:

© 2021. American Geophysical Union. All Rights Reserved.

Zhang, J., Yuan, Q., Liu, L., Wang, Y., Zhang, Y., Xu, L., et al. (2021). Transregional transport of haze particles from the North China Plain to Yangtze River Delta during winter. *Journal of Geophysical Research: Atmospheres*, 126, e2020JD033778.

To view the published open abstract, go to: <https://doi.org/10.1029/2020JD033778>

General rights

Unless a licence is specified above, all rights (including copyright and moral rights) in this document are retained by the authors and/or the copyright holders. The express permission of the copyright holder must be obtained for any use of this material other than for purposes permitted by law.

- Users may freely distribute the URL that is used to identify this publication.
- Users may download and/or print one copy of the publication from the University of Birmingham research portal for the purpose of private study or non-commercial research.
- User may use extracts from the document in line with the concept of 'fair dealing' under the Copyright, Designs and Patents Act 1988 (?)
- Users may not further distribute the material nor use it for the purposes of commercial gain.

Where a licence is displayed above, please note the terms and conditions of the licence govern your use of this document.

When citing, please reference the published version.

Take down policy

While the University of Birmingham exercises care and attention in making items available there are rare occasions when an item has been uploaded in error or has been deemed to be commercially or otherwise sensitive.

If you believe that this is the case for this document, please contact UBIRA@lists.bham.ac.uk providing details and we will remove access to the work immediately and investigate.

JGR Atmospheres

RESEARCH ARTICLE

10.1029/2020JD033778

Key Points:

- Abundant primary brown carbon in the North China Plain (NCP) can transport over 1,000 km to influence climate and human health in East China
- The aging of haze particles in the trans-regional transport significantly transformed their mixing structures and hygroscopic properties
- Residential coal burning in the rural areas of the NCP is the main source of these primary brown carbon aerosols

Supporting Information:

Supporting Information may be found in the online version of this article.

Correspondence to:







W. Li,
liweijun@zju.edu.cn

Citation:

Zhang, J., Yuan, Q., Liu, L., Wang, Y., Zhang, Y., Xu, L., et al. (2021). Trans-regional transport of haze particles from the North China Plain to Yangtze River Delta during winter. *Journal of Geophysical Research: Atmospheres*, 126, e2020JD033778. <https://doi.org/10.1029/2020JD033778>

Received 27 AUG 2020
 Accepted 22 MAR 2021

Trans-Regional Transport of Haze Particles From the North China Plain to Yangtze River Delta During Winter

Jian Zhang¹, Qi Yuan¹, Lei Liu¹ , Yuanyuan Wang¹, Yinxiao Zhang¹, Liang Xu¹, Yuner Pang¹, Yanhong Zhu¹, Hongya Niu², Longyi Shao³ , Shushen Yang⁴, Hang Liu⁵ , Xiaole Pan⁵ , Zongbo Shi⁶ , Min Hu⁷, Pingqing Fu⁸, and Weijun Li¹ 

¹Department of Atmospheric Sciences, School of Earth Sciences, Zhejiang University, Hangzhou, China, ²Key Laboratory of Resource Exploration Research of Hebei Province, Hebei University of Engineering, Handan, China, ³State Key Laboratory of Coal Resources and Safe Mining, China University of Mining and Technology, Beijing, China, ⁴School of Energy and Environment, Zhongyuan University of Technology, Zhengzhou, China, ⁵State Key Laboratory of Atmospheric Boundary Layer Physics and Atmospheric Chemistry, Institute of Atmospheric Physics, Chinese Academy of Sciences, Beijing, China, ⁶School of Geography, Earth and Environmental Sciences, University of Birmingham, Birmingham, UK, ⁷State Key Joint Laboratory of Environmental Simulation and Pollution Control, College of Environmental Sciences and Engineering, Peking University, Beijing, China, ⁸Institute of Surface-Earth System Science, School of Earth System Science, Tianjin University, Tianjin, China

Abstract According to atmospheric modeling and satellite observations, cold fronts can cause trans-regional transport (TRT) of haze particles from the North China Plain (NCP) to Yangtze River Delta (YRD) in winter. However, compositions and aging of haze aerosols during the TRT have not been studied. We showed the TRT PM_{2.5} dominated by organic matter (OM) (30%) and secondary inorganic ions (36%) in the NCP and 29% and 60% in the YRD. Following the TRT, abundant spherical primary OM particles (i.e., tarballs) (71% by number) mainly from residential coal burning in rural areas of the NCP unexpectedly occurred in the YRD. The inert tarballs display similar sizes (~300 nm) and O/C ratios (~0.15), but the mixture of nitrate, sulfate, and secondary OM as the coatings completely convert the hydrophobic tarballs into hydrophilic ones in the TRT. The aging and transport of tarballs from the NCP to YRD further indicate that the TRT not only brought various trace gases (e.g., CO, SO₂, NO_x, and VOCs) but also carried large numbers of nanosized primary particles (e.g., tarball, metal, fly ash, and soot) with secondary coatings over 1,000 km. The findings suggest that these many nanosized tarballs containing brown carbon and highly toxic species in the NCP influence regional climate and human health in northern and eastern China, which needs more attention. Although the NCP and YRD have different energy consumption structures in winter and are two isolated administrative regions, we emphasize the need for a coordinated cross-regional emission reduction strategy for TRT haze control.

Plain Language Summary The North China Plain (NCP) and Yangtze River Delta (YRD) are two isolated administrative regions in China with developed economies and serious regional haze pollution during winter. There are different particle sources in the NCP and YRD in winter, in particular for the abundant coal burning for heating and cooking in the NCP but not in the YRD. Recently, it has been found that cold air can cause trans-regional transport (TRT) of haze particles from the NCP to YRD in winter and further induces regional haze pollution in the YRD. However, there is no detailed information on the fine TRT haze particles. Here we raise several questions about the fine particles: What kinds of fine particles can be transported from the NCP to YRD? How are these particles changed during their TRT? The answers are important for evaluating the impacts of air pollution between the two large city-clusters on human health and climate. Therefore, we conducted field campaigns and analyzed compositions and aging of fine haze particles during their TRT. This study not only provides critical information about the TRT haze particles but also insights to the future coordination of air pollution control between the NCP and YRD in winter.

1. Introduction

Because of the rapid development of urbanization and industrialization and rise of economy, China has frequently experienced haze pollution. These haze pollution events profoundly affect human health, such as

respiratory system and heart (Lelieveld et al., 2020); climate, such as temperature and precipitation (Suzuki & Takemura, 2019); and ecosystem, such as growth of plankton in remote ocean areas (Li, Xu, et al., 2017). Although the Chinese government has adopted a series of control measures (e.g., the 12th Five-Year Plan for Air Pollution Control in Key Areas and Air Pollution Prevention and Control Action Plan), some regional haze pollution events still occur in winter owing to adverse meteorological conditions (e.g., low wind speed and high relative humidity (RH)), relatively high emissions from household heating, vehicle exhausts, and industry activities, regional or long-range transport of air pollutants, and secondary aerosol formation (J. Liu et al., 2016; X. Pan et al., 2019; Shao et al., 2019; Yao et al., 2018; F. Zhang et al., 2020; Zhang, Liu, Xu, et al., 2020; G. J. Zheng et al., 2015; H. Zheng et al., 2019; Zhong et al., 2019).

The North China Plain (NCP) and the Yangtze River Delta (YRD) are two developed regions in China with serious haze pollution (Guo et al., 2014; Li, Wang, et al., 2019). There are two large city-clusters, with Beijing and Shanghai being the political and economic centers in the NCP and YRD. The statistical data show that nearly 50% of China's total population lives in the NCP and YRD and that approximately one-half of fossil fuel in China is consumed for industrial, residential, and vehicular activities in these two regions (all data from National Bureau of Statistics of China, <http://data.stats.gov.cn/index.htm>, last access: December 9, 2020). Therefore, the regional haze pollution in the NCP and YRD is a major world concern (Cheng et al., 2013; Lyu et al., 2019; S. Zhai et al., 2018; Y.-L. Zhang et al., 2018; Zhong et al., 2019). The previous studies suggested that regional winter haze events in the NCP were formed by accumulation of air pollutants under stable meteorological conditions (C. Liu et al., 2017; X. J. Zhao et al., 2013) and were further deteriorated by massive formation of secondary aerosols from their gaseous precursors (e.g., SO₂, NO₂, and volatile organic compounds (VOCs)) (J. Wang et al., 2020; Xue et al., 2019; G. J. Zheng et al., 2015) and two-way feedback between haze aerosols and meteorological conditions (Z. Li et al., 2017; Wang, Shi, et al., 2015; Zhong et al., 2019). Finally, these haze events in the NCP are terminated by strong northerly or northwesterly winds (i.e., cold fronts). As a result, air pollutants in haze events in the NCP are rapidly transported to downwind regions such as the YRD (Kang et al., 2019) or East China Sea (F. Wang et al., 2016). To date, most of studies have focused on physicochemical characteristics of aerosol particles and regional haze formation in the NCP or the YRD as two isolated regions (Cheng et al., 2013; Ge et al., 2018; Herrmann et al., 2014; Lyu et al., 2019; Wang, An, et al., 2014; S. Zhai et al., 2018). There are only a small number of studies concerning the trans-regional transport (TRT) of air pollutants from the NCP to the YRD through atmospheric models (X. Huang et al., 2020; Kang et al., 2019; Li, Wang, et al., 2019). However, it is essential to study the TRT of fine particles because of its large-scale potential impacts on human health, climate, and ecosystem (Conway et al., 2019; Shrivastava et al., 2017; Yue et al., 2019; Zhao & Garrett, 2015).

Many mountains (e.g., Taihang Mountains, Ta-pieh Mountains, and Mount Huang) lie to the west of the NCP and YRD, and the Bohai Sea, Yellow Sea, and East China Sea are to the east of the NCP and YRD (Figure 1a). There are no obvious high mountains barriers between the NCP and the YRD, although the Yangtze River separates northern and eastern China into two large isolated administrative regions, with the NCP as the northern part and the YRD as the southern part (Figure 1a). Therefore, it is reasonable to observe the TRT haze events from the NCP to YRD in winter because of cold fronts (He et al., 2018; Kang et al., 2019). Although a few studies have observed some TRT haze events from the NCP to YRD during winter, they only analyzed the impact of weather system on TRT by weather patterns (He et al., 2018; Hou et al., 2020; J. Li et al., 2019; Shu et al., 2017) or variations of components and geographical contribution of PM_{2.5} in the YRD during TRT by bulk analysis (Li, Wang, et al., 2019; Ming et al., 2017), radiosonde observation (Zhong et al., 2019), lidar measurement (T. Sun et al., 2018), and model simulation (X. Huang et al., 2020; Kang et al., 2019; Li, Huang, et al., 2012; Ming et al., 2017). For example, He et al. (2018) suggested that during winter, high frequency of cold fronts at 21%–41% can transport regional haze events occurring in the NCP into the downwind YRD; Kang et al. (2019) further found that the cold fronts bringing air pollutants from the NCP can increase YRD PM_{2.5} concentration from ~70 to >200 μg m⁻³ within 8 h based on the meteorological model and ground-based observations. When a TRT haze event from the NCP to YRD occurred, it can cause YRD PM₁₀ mass concentration contributed from the TRT of the NCP to be approximately twice higher than that from the local YRD emission (Li, Huang, et al., 2012). However, field observations of the TRT haze events have not been conducted to provide more specific evidences of chemical compositions and mixing states of fine particles during their transports from the NCP to YRD, which would contribute to understanding how haze particles are formed, age, and die during the TRT.

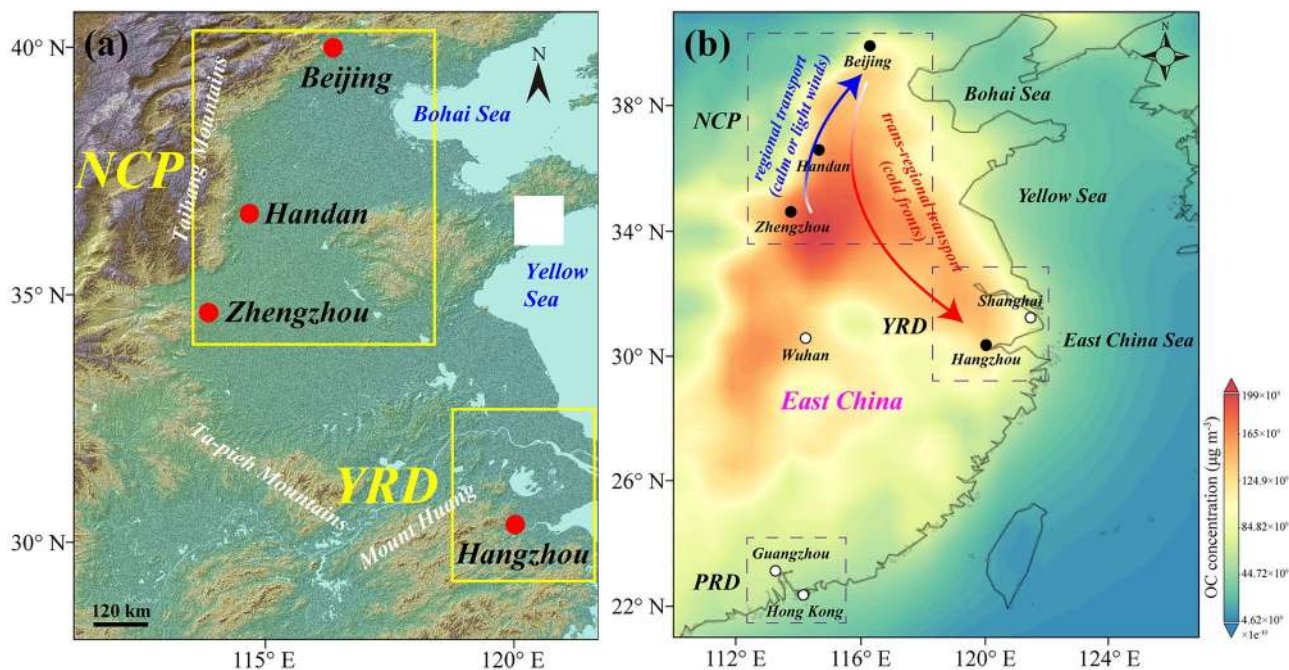


Figure 1. Sampling sites and schematic diagram of the trans-regional transport (TRT) haze events in East China. (a) Geographic locations of four sampling sites (i.e., Beijing, Handan, Zhengzhou, and Hangzhou) in the North China Plain (NCP) and the Yangtze River Delta (YRD). (b) Schematic diagram of the TRT haze events in East China during winter with spatial distribution of monthly averaged organic carbon surface mass concentration during December 2017. The white block in panel (a) represents that data are missed. The spatial distribution of organic carbon concentration in panel (b) is derived from the Modern-Era Retrospective Analysis for Research and Applications, Version 2 (MERRA-2) model (<https://giovanni.gsfc.nasa.gov/giovanni/>, last access: May 10, 2020).

To better study the variations of chemical compositions and aging characteristics of haze particles during the TRT from the NCP to YRD, we performed field observations in four cities (i.e., Beijing, Handan, Zhengzhou, and Hangzhou) located in the NCP and YRD in December 2017. A typical TRT haze event from the NCP to YRD covering these four cities occurred from December 26 to 31, 2017. This study investigated the compositions of $PM_{2.5}$, mixing structures of individual particles, and hygroscopic behavior of haze aerosols at the four sampling sites during the TRT haze event.

2. Observations and Methods

2.1. Sampling Sites and Sample Collection

Four sampling sites in the urban areas of Beijing, Handan, and Zhengzhou cities of the NCP and Hangzhou city of the YRD were selected to study the TRT haze event from the NCP to the YRD in winter (Figure 1a).

Beijing city ($40^{\circ}N$, $116.35^{\circ}E$) is located in the northern part of the NCP (Figure 1a). Although the average $PM_{2.5}$ concentration ($52 \mu g m^{-3}$) in Beijing in winter of 2017 is lower than the Grade II national ambient air quality standard value ($75 \mu g m^{-3}$) (Table S1), heavy hazes still occurred in Beijing in winter under adverse meteorological conditions through secondary transformation of aerosols and regional transport from the central and southern parts of the NCP (G. J. Zheng et al., 2015).

Handan ($36.58^{\circ}N$, $114.51^{\circ}E$) and Zhengzhou ($34.59^{\circ}N$, $113.69^{\circ}E$) cities are located in the central and southern parts of the NCP (Figure 1a). There are intense pollutant emissions in these areas, which mainly include many heavy industrial activities around these two cities (e.g., steel and nonferrous metals factories, cement plants, glass factories, and coal-fired plants) and residential coal burning for heating and cooking in thousands of rural villages in the NCP because of quite low temperature during winter (J. Liu et al., 2016). The high emissions can cause regional heavy haze pollution in the NCP in winter (S. Liu et al., 2018; Yang et al., 2018), with the average $PM_{2.5}$ concentrations of 105 and $91 \mu g m^{-3}$ in winter of 2017 which are higher than the Grade II standard value of $75 \mu g m^{-3}$ (Table S1).

Hangzhou city (30.31°N, 120.09°E) is a typical megacity in the YRD and is located in the south-central part of the YRD (Figure 1a). Its air quality can be influenced by the long-range transported hazes from the NCP under strong cold fronts (Li, Wang, et al., 2019). The average $PM_{2.5}$ concentration was $63 \mu\text{g m}^{-3}$ during winter in 2017 in Hangzhou (Table S1), which is lower than the Grade II standard value of $75 \mu\text{g m}^{-3}$. Regional haze events frequently appeared in the YRD in winter because of regional emissions from urban vehicle exhausts and industrial activities (Liu, Zhang, et al., 2020; Xu, Zhang, et al., 2020), as well as the TRT of air pollutants from the NCP (Li, Wang, et al., 2019; Ming et al., 2017). Compared with the NCP, there are no coal-fired heating activities in villages and central heating in urban areas in the YRD during winter.

Ambient $PM_{2.5}$ and individual aerosol particles were collected on 90 mm preheated (600°C for 4 h) quartz filters (Whatman, UK) using medium volume samplers including $PM_{2.5}$ impactors (Wuhan Tianhong Inc., TH-16A, 100 L min^{-1}) and transmission electron microscopy (TEM) grids and silicon wafers using DKL-2 samplers (Genstar Inc., 1 L min^{-1}) at the four sampling sites. $PM_{2.5}$ samples, including the blank samples (in the same collection way but no pumping), were collected twice a day from 8:30 (local time) to 20:00 (named daytime (DT)) and from 20:30 to 8:00 on next day (named nighttime (NT)). The blank samples were used to correct the ambient $PM_{2.5}$ and its chemical composition concentrations. Individual particle samples were collected four times a day at 0:00–3:00 (local time), 7:00–10:00, 12:00–15:00, and 18:00–21:00 with unstable sampling durations from 30 s to 8 min based on $PM_{2.5}$ concentrations. During the TRT haze event, although intermittent rain occurred at the sampling sites and caused six $PM_{2.5}$ samples before and after the TRT process to be missed, samples during the TRT process were not influenced. After the sampling, $PM_{2.5}$ samples were immediately stored in -20°C refrigerators and individual particle samples were sealed in dry, clean, and airtight containers until next laboratory analyses.

Meteorological fields, including wind speed and direction, temperature, geopotential height, and RH at 1,000 and 900 hPa in East China were obtained based on the FNL data ($1^\circ \times 1^\circ$) from the National Centers for Environmental Prediction (NCEP) (<https://rda.ucar.edu/datasets/ds083.2/>, last access: April 30, 2020). Hourly meteorological parameters (i.e., wind speed and direction, RH, and temperature) and concentrations of $PM_{2.5}$ and CO were derived from the nearest monitoring stations (<https://www.aqistudy.cn/>, last access: April 30, 2020).

2.2. $PM_{2.5}$ Chemical Composition Analyses

Quartz filters were weighted using a high-precision digital balance (Sartorius ME 5-F) with 0.001 mg of reading precision before and after sampling in a room with the following conditions: a temperature of $20^\circ\text{C} \pm 1^\circ\text{C}$ and an RH of $50\% \pm 2\%$. The mass concentrations of DT and NT $PM_{2.5}$ during the sampling period were further calculated based on the weight differences of quartz filters and sampling volumes. Although there is a $11\% \pm 7\%$ deviation between the weighted $PM_{2.5}$ concentrations and $PM_{2.5}$ concentrations from the nearby air quality monitoring stations, their variations during the TRT haze event are same. Therefore, the weighted $PM_{2.5}$ concentrations can be used to reflect the TRT haze formation from the NCP to the YRD.

$PM_{2.5}$ samples were analyzed to obtain water-soluble ions (i.e., SO_4^{2-} , NO_3^- , NH_4^+ , Ca^{2+} , Mg^{2+} , K^+ , Na^+ , Cl^- , and F^-) by an ion chromatography system (Dionex ICs-90, USA), organic carbon (OC) and elemental carbon (EC) by an OC-EC analyzer (Sunset Laboratory Inc., USA), and trace metals (i.e., V, Cr, Mn, Fe, Co, Ni, Cu, Zn, Ge, Mo, Tc, Rh, Cd, Ag, In, Sn, Sb, Ba, Tb, Lu, Tl, Pb, Bi, Th, and U) by inductively coupled plasma mass spectrometry (ICP-MS, Agilent 7500ce). The detailed experimental processes were provided in the previous studies (Y. Pan et al., 2013; Zhang, Liu, Wang, et al., 2017; Zhu et al., 2020). Concentrations of organic matter (OM) were obtained by multiplying OC by a factor of 1.91, as reported by Xing et al. (2013).

2.3. TEM-EDS Analysis

Individual aerosol particles collected on TEM grids were analyzed using a TEM equipped with energy-dispersive X-ray spectrometry (EDS) (JEOL, JEM-2100). TEM-EDS analysis can obtain physical (e.g., morphology and mixing structure) and chemical (e.g., elemental composition and ratio of elements) properties of

individual particles. Each EDS spectra collection time is controlled within 30 s to reduce potential X-ray damage and ensure sufficient signal intensity to individual particles. In EDS spectra, copper (Cu) is excluded because of the effect from the Cu TEM grids and carbon (C) may be overestimated for thin particles since the substrate is C film. Here, we collected C and O from thick OM particles to calculate the O/C ratio which can indicate the oxidation degree of organic particles. In total, 1,087 particles in Beijing, 1,176 particles in Handan, 1,321 particles in Zhengzhou, and 963 particles in Hangzhou were analyzed.

The area, perimeter, shape factor, and equivalent circle diameter (ECD) of each particle in TEM images were measured using an image analysis software (Radius, EMSIS GmbH, Germany). The shape factor can be used to show morphological characteristics of individual particles. When the shape factor is closer to 1 (the maximum value), the particle is rounder (Xu, Fukushima, et al., 2020).

2.4. Geographic Source Analyses

The concentration-weighted trajectory (CWT) analysis based on backward trajectory can be employed to estimate the contribution of air pollutants from different regions (H. Zheng et al., 2019). Before the CWT analysis, air mass backward trajectory needs to be calculated. In this study, 72 h of air mass backward trajectories with one-hour resolution before arriving at the four sampling sites at 500 m a.g.l. were calculated based on the wind data sets from the Nation Oceanic Atmospheric Administration (NOAA) (<ftp://arlftp.arlhq.noaa.gov/pub/archives/gdas1>, last access: March 31, 2020). A user-friendly Igor-based tool “ZeFir” developed by Petit et al. (2017) was utilized for the CWT analysis. The region covered by the trajectories of CWT consists of thousands of cells with a resolution of $0.4^\circ \times 0.4^\circ$. The CWT was simulated according to the following equation:

$$C_{ij} = \frac{1}{\sum_{k=1}^N \tau_{ijk}} \sum_{k=1}^N C_k \tau_{ijk} \quad (1)$$

where C_{ij} is the average weighted concentration in a grid cell (i, j); C_k is the measured concentration of pollutant observed on the arrival of trajectory k ; τ_{ijk} is the number of trajectory endpoints in the grid cell (i, j) associated with the C_k sample; N is the number of samples that have trajectory endpoints in the grid cell (i, j). To further improve the accuracy of the CWT analysis, a weighing function in “ZeFir,” as shown in Equation 2, was applied to the CWT calculation.

$$W = \begin{cases} 1 & \text{for } \log(n+1) \geq 0.85 \times \max_{\log(n+1)} \\ 0.725 & \text{for } 0.6 \times \max_{\log(n+1)} \leq \log(n+1) < 0.85 \times \max_{\log(n+1)} \\ 0.475 & \text{for } 0.35 \times \max_{\log(n+1)} \leq \log(n+1) < 0.6 \times \max_{\log(n+1)} \\ 0.175 & \text{for } \log(n+1) < 0.35 \times \max_{\log(n+1)} \end{cases} \quad (2)$$

$\log(n+1)$ represents the density of trajectory.

To further verify the geographic sources and transport of haze particles, the Lagrangian particle dispersion model FLEXPART was applied (Stohl et al., 2005). The FLEXPART model computed backward footprints of particles on the basis of considering atmospheric turbulence and convection, particle deposition, and reactions with hydroxyl radicals (Eckhardt et al., 2009). In this study, this model was run by hourly meteorological data with a $0.5^\circ \times 0.5^\circ$ resolution and 37 vertical levels derived from the NCEP (<https://rda.ucar.edu/datasets/ds094.0/>, last access: April 30, 2020). Twenty-thousand particles at the sampling site were released in the FLEXPART model to determine the geographic sources of haze particles more accurately. Finally, 72 h of horizontal and vertical backward footprints of haze particles with particle residence time and backward trajectory of air mass were obtained. More details regarding the FLEXPART model were reported by Stohl et al. (2005).

2.5. Hygroscopic Experiments

An individual particle hygroscopic (IPH) system is applied to observe the hygroscopic properties of individual haze particles from the NCP to YRD. The experimental steps of the IPH system are as follows: (1) dry and wet N₂ gases were introduced into a chamber through a mass flow controller; (2) a TEM grid or silicon wafer was placed into an environmental microscopic cell (Gen-RH Mcell, UK), where the RH can be changed by dry and wet N₂ gases and kept at a temperature of 20°C by a constant temp bath (DC-0506); (3) images of individual particles were taken at different RH values via an optical microscope (Olympus BX51M, Japan) equipped with a camera (Canon 650D). The IPH system was successfully used to investigate the hygroscopic properties of individual particles collected on TEM grids and silicon wafers (Chi et al., 2015; J. Sun et al., 2018; Zhang, Yuan, et al., 2018). In this study, hygroscopic growth of individual haze particles collected at the four sampling sites of the NCP to YRD was obtained at RH values of 3%–93%. A parameter, that is, “growth factor (GF),” that can quantify particle size change was used to evaluate the hygroscopic characteristics of individual haze particles. The GF calculation is as follows:

$$GF_k = \frac{1}{n} \sum_{i=1}^n \frac{D_{ik}}{D_{i0}} \quad (3)$$

where GF_k is the average GF of individual haze particles at each sampling site at $k\%$ RH; D_{ik} is the ECD of particle i at $k\%$ RH; D_{i0} is the ECD of particle i at 3% RH; n is the number of analyzed particles.

3. Identification of Trans-Regional Transport Haze Event

Figures S1a–S1e show a regional heavy haze event with continuous haze movement from the NCP to the YRD along with a cold front from December 26 to 31. Based on the variations of PM_{2.5} mass concentrations and visibility at the four sampling sites, we found that haze pollution (PM_{2.5} ≥ 75 μg m⁻³ and visibility < 10 km) gradually formed in the NCP during the period of 26–29 December, and then it was cleared (PM_{2.5} < 75 μg m⁻³ and visibility > 10 km) on 30 December (Figures 2e and S2a). Consequently, a regional haze event suddenly occurred in the YRD under the condition of strong northwest winds during the period of 30–31 December (Figures 2d, 2e and S2a). We noticed that wind played an important role in the TRT haze event, which is consistent with other studies on the sudden formation of haze in the YRD (X. Huang et al., 2020; Kang et al., 2019; Li, Wang, et al., 2019). Figures 2a–2d show that low wind speeds at ~1.4 m s⁻¹ prevailed at the four sampling sites before December 30, suggesting that there was no TRT haze event from the NCP to the YRD. Following a cold front occurring in the NCP on December 30, we noticed that the weak southerly winds at ~0.5 m s⁻¹ quickly changed to strong northwest winds at ~4.7 m s⁻¹ within 2 h in Beijing, Handan, and Zhengzhou (Figures 2a–2c). As a result, the hourly PM_{2.5} concentrations quickly dropped from 253, 422, and 300 μg m⁻³ to 15, 56, and 38 μg m⁻³ in Beijing, Handan, and Zhengzhou, respectively, on December 30 (Figure 2e). Four hours after the haze pollution disappeared in the NCP, we found that the PM_{2.5} concentration quickly increased from 35 to 318 μg m⁻³ under strong northwest winds at ~3.9 m s⁻¹ in Hangzhou in the YRD on December 30 (Figures 2d and 2e). The meteorological model provides wind fields at both 1,000 (surface) and 900 hPa (~1,000 m a.g.l.) in East China (Figures 3a, 3b, 4a, and 4b). The wind fields show coincident results with the observed wind data, that is, that strong northwest winds prevailed on December 30 compared with weak winds before December 30 in the NCP and the YRD. In addition, with the occurrence of cold front, temperature at the four sampling sites largely decreased from 10°C ± 3°C to -3°C ± 3°C (Figure S3b).

The CWT analysis clearly shows that high PM_{2.5} concentrations in the YRD during the period of December 30–31, mainly originated from the NCP and the TRT contribution from the NCP reached ~36.4% (Figure 4c). Furthermore, we ran the FLEXPART model at Hangzhou sampling site and found that haze particles in the YRD were indeed sourced from the TRT of the NCP (Figure 4d). These results firmly demonstrate that the regional haze in the NCP was transported to downwind areas by a cold front and invaded the YRD during the period of December 30–31 (Figures S1a–S1e). Kang et al. (2019) investigated the weather in the whole wintertime of 2014 and found that at least 13 TRT haze events from the NCP to the YRD were induced by strong northerly and northwesterly winds. As a result, our analysis shows that a regional haze

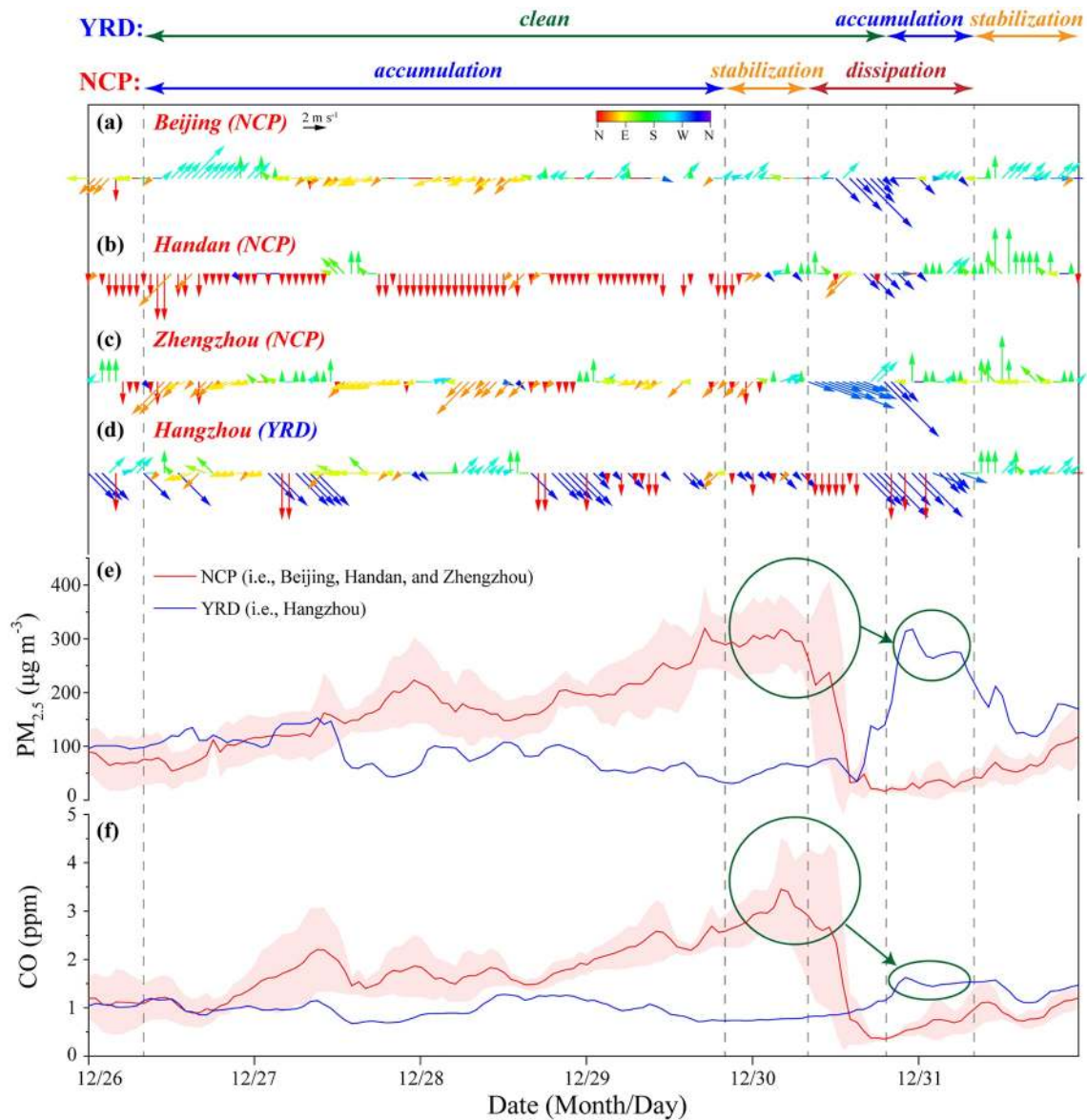


Figure 2. Times series of wind data and PM_{2.5} and CO concentrations in Beijing, Handan, Zhengzhou, and Hangzhou during the TRT haze event from the NCP to YRD. (a–d) Wind speed and direction. (e) PM_{2.5}. (f) CO. In panels (e–f), the green circles represent the PM_{2.5} and CO concentration peaks and the green arrows indicate the variation in the concentration peaks following the TRT from the NCP to the YRD.

event gradually formed in the NCP and then turned into a typical TRT haze event following a cold front movement from the NCP to the YRD during the period of December 26–31.

Based on the variation in wind and PM_{2.5} concentration, the TRT haze event was divided into three stages in both the NCP and the YRD (Table S2). The three stages in the NCP are as follows: Accumulation stage from 26 DT to 29 DT December with weak winds and continuously increased PM_{2.5}; stabilization stage on 29 NT with light air and persistently high PM_{2.5}; and dissipation stage from 30 DT to 30 NT December with strong northwest winds and rapidly decreased PM_{2.5} (Figures 2a, 2e, and S2a). Similarly, there are three stages in the YRD: clean stage from 26 DT to 30 DT with weak winds and low PM_{2.5}; accumulation stage on 30 NT December with strong northwest winds and rapidly increased PM_{2.5}; stabilization stage from 31 DT to 31 NT December with weak winds and high PM_{2.5} (Figures 2a, 2e, and S2a). Because we mainly studied the TRT haze event from the NCP to the YRD, the accumulation, stabilization, and dissipation stages in the NCP and clean and accumulation stages in the YRD were primarily investigated.

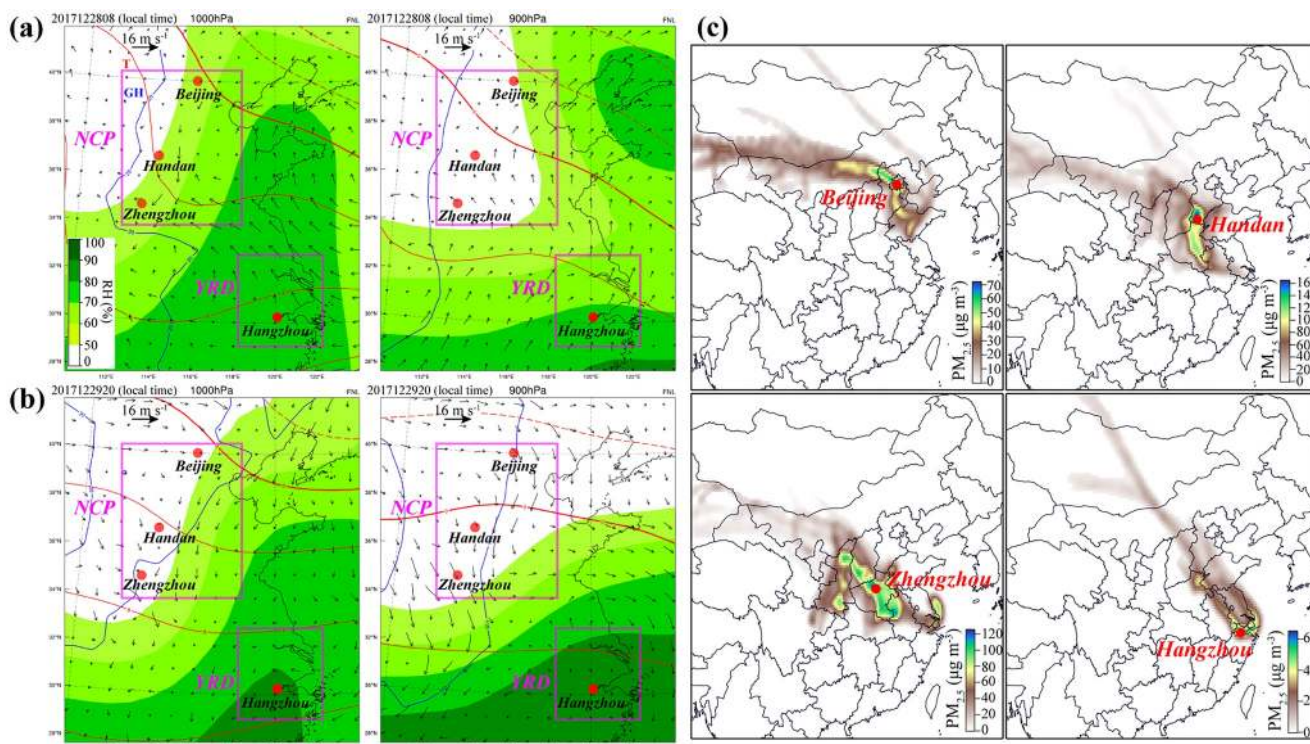


Figure 3. Meteorological fields and potential geographical origins of PM_{2.5} before December 30. (a–b) Meteorological fields covering the NCP and YRD at 1,000 and 900 hPa before December 30. (c) Concentration-weighted trajectory (CWT) plots of PM_{2.5} before arriving in Beijing, Handan, Zhengzhou, and Hangzhou before December 30. The red lines, blue lines, and green fillings in panels (a) and (b) represent temperature (*T*), geopotential height (*GH*), and relative humidity (*RH*).

4. Results and Discussion

4.1. Meteorology and PM_{2.5} Compositions

Figures S2a–S2e show that the changes in PM_{2.5} concentrations and their chemical compositions appeared to have similar trends among Beijing, Handan, and Zhengzhou of the NCP during the TRT haze event. Winds remained at $\sim 1.3 \text{ m s}^{-1}$ and the average RH increased from 31% to 73% in the NCP during the accumulation stage (Figures 2a, 2c, and S3a). During the accumulation stage, the semidiurnal PM_{2.5} and CO concentrations gradually increased from $136 \mu\text{g m}^{-3}$ and 1.1 ppm to $302 \mu\text{g m}^{-3}$ and 2.4 ppm in the NCP, with the average concentrations at $218 \mu\text{g m}^{-3}$ and 1.8 ppm (Figures 2f and 5). OM and secondary inorganic ions (SNA, the sum of SO_4^{2-} , NO_3^- , and NH_4^+) dominated PM_{2.5} in the NCP during the accumulation stage. Figures 5 and S2b–S2d show that the average OM and SNA concentrations were 72 and $67 \mu\text{g m}^{-3}$ in the NCP based on 68 and $50 \mu\text{g m}^{-3}$ in Beijing, 86 and $83 \mu\text{g m}^{-3}$ in Handan, and 62 and $67 \mu\text{g m}^{-3}$ in Zhengzhou. Following the further aggravation of meteorological conditions (weak winds at $\sim 0.8 \text{ m s}^{-1}$ and high RH at 80%), the regional haze in the NCP evolved into the stabilization stage from the accumulation stage (Figures 2a, 2c, and S3a). The average PM_{2.5} concentration increased from $218 \mu\text{g m}^{-3}$ during the accumulation stage to $313 \mu\text{g m}^{-3}$ during the stabilization stage in the NCP (Figure 5). The hourly CO concentration in the NCP reached its maximum value at 3.5 ppm during the stabilization stage, with an average value of 3.1 ppm (Figure 2f). Figure 5 shows that OM and SNA concentrations increased from 72 and $67 \mu\text{g m}^{-3}$ to 93 and $111 \mu\text{g m}^{-3}$, respectively, in the NCP when the haze event from the accumulation stage evolved into the stabilization stage. It should be noted that SNA concentrations strikingly increased by 60%–138% during the period of 27 NT–29 NT, with RH at 62%–88% following the regional haze accumulation and stabilization in the NCP (Figures S2b–S2d and S3a). Similar results showing that massive production of secondary aerosols under high RH (>60%) induced severe haze formation in North China in winter have been documented well (G. Wang et al., 2016; J. Wang et al., 2020; G. J. Zheng et al., 2015). In the NCP, the

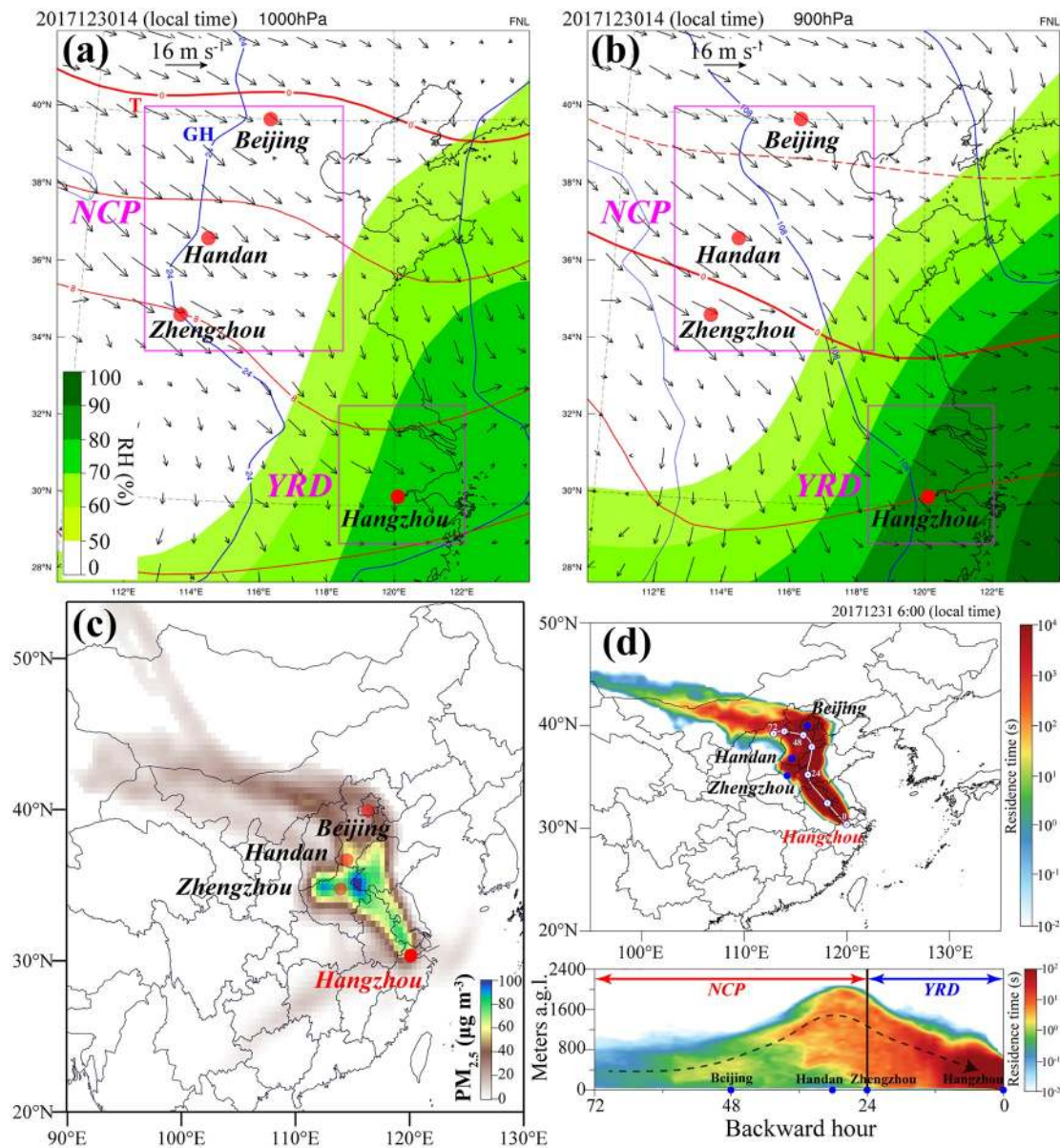


Figure 4. Meteorological fields and potential geographical origins of PM_{2.5} and haze particles during December 30–31. (a–b) Meteorological fields covering the NCP and YRD at 1,000 and 900 hPa on December 30. (c) CWT plots of PM_{2.5} before arriving in Hangzhou during December 30–31. (d) 72 h backward footprint analysis of particle transport using the FLEXPART model in Hangzhou at 06:00 (local time) on December 31.

period from the accumulation stage to the stabilization stage took four days to accumulate and regionally transport large amounts of anthropogenic air pollutants along the north-south Taihang Mountains (Figures 3a–3c).

During the same period, the YRD had better air quality when a regional haze formed in the NCP (Figures 2e and S2a). This converse phenomenon between the YRD and the NCP has often been observed during winter (J. Li et al., 2019; Li, Wang, et al., 2019; Shi et al., 2020). Indeed, we noticed that PM_{2.5} and CO concentrations remained at a low level of $82 \mu\text{g m}^{-3}$ and 0.9 ppm, respectively, in the YRD during the period of 26 DT–30 DT December, although wind speeds were low at $\sim 1.4 \text{ m s}^{-1}$ (Figures 2d–2f). Obviously, this period was the clean stage in the YRD. The average OM and SNA concentrations were 25 and $31 \mu\text{g m}^{-3}$ during the clean stage in the YRD (Figure 5).

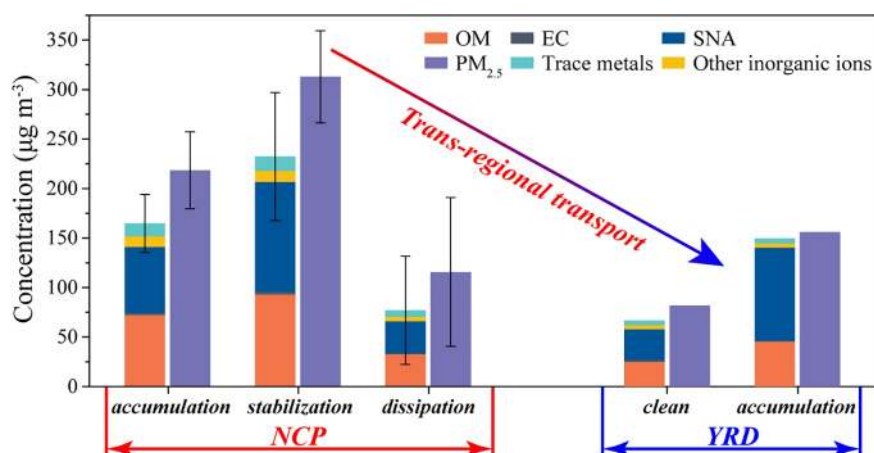


Figure 5. Mass concentrations of PM_{2.5} and organic matter (OM), elemental carbon (EC), secondary inorganic ions (SNA, i.e., SO₄²⁻, NO₃⁻, and NH₄⁺), other inorganic ions (i.e., Ca²⁺, Mg²⁺, K⁺, Na⁺, Cl⁻, and F⁻), and trace metals in PM_{2.5} during the TRT haze event from the NCP to YRD.

Figures 2a–2c and 2e show that the high concentrations of PM_{2.5} in the NCP rapidly dropped from 253–422 $\mu\text{g m}^{-3}$ to 15–56 $\mu\text{g m}^{-3}$ when the weak southerly winds at $\sim 0.5 \text{ m s}^{-1}$ changed to strong northwest winds at $\sim 4.7 \text{ m s}^{-1}$. The regional severe haze in the NCP was completely swept within 6 h (Figure 2e). During the same period, we observed that the YRD air quality became worse (Figure 2e). Figures 5 and 2f show that the average concentrations of PM_{2.5} and CO in the NCP together decreased from 313 $\mu\text{g m}^{-3}$ and 3.1 ppm during the stabilization stage to 116 $\mu\text{g m}^{-3}$ and 1.0 ppm during the dissipation stage, but the concentrations of PM_{2.5} and CO in the YRD dramatically increased from 82 $\mu\text{g m}^{-3}$ and 0.9 ppm during the clean stage to 156 $\mu\text{g m}^{-3}$ and 1.5 ppm during the accumulation stage. CO as one tracer of primary combustion emission (Y. J. Li et al., 2015), it had positive correlations with PM_{2.5} at the four sampling sites ($0.22 \leq R^2 \leq 0.96$) (Figures S4a–S4d), suggesting that primary combustion constantly contributed haze particles during the TRT haze event from the NCP to the YRD. Meanwhile, we found that OM and SNA concentrations distinctly increased from 25 and 31 $\mu\text{g m}^{-3}$ during the clean stage to 45 and 94 $\mu\text{g m}^{-3}$ during the accumulation stage in the YRD (Figure 5). Notably, nitrates in PM_{2.5} largely increased from 17 $\mu\text{g m}^{-3}$ during the clean stage to 50 $\mu\text{g m}^{-3}$ during the accumulation stage in the YRD compared to sulfates and ammonium (Figure S2e). Total trace metals, including Fe, Mn, Cr, Pb, and Zn, also increased from 4.9 $\mu\text{g m}^{-3}$ during the clean stage to 5.2 $\mu\text{g m}^{-3}$ during the accumulation stage in the YRD following the TRT from the NCP (Figure 5). In summary, regional haze pollution formed in the YRD in the accumulation stage when the NCP was in the dissipation stage. Obviously, the meteorological fields, CWT analysis, and FLEXPART model all prove that the converse phenomenon between the YRD and NCP is attributed to the TRT haze events in East China (Figures 4a–4d). Therefore, the variation in chemical compositions of aerosol particles during the TRT haze events should be paid more attention.

4.2. Classification of Individual Particles

TEM-EDS analysis obtained the morphology, mixing structures, and elemental compositions of individual particles (Figures 6a–6i). In consequence, four basic major types of aerosol components in fine particles are classified as OM, SNA, soot, and metal/fly ash (Figures 6a–6i).

SNA particles, also called secondary inorganic aerosols, are mainly comprised of S, O, and N elements (Figure 6h) and generally are the mixture of (NH₄)₂SO₄ and NH₄NO₃ (Li, Sun, et al., 2016). Individual soot particles, also called black carbon, are aggregation of many carbonaceous spheres (Figures 6c, 6d, and 6f) and mainly contain C and minor O (Figure 6h). Metal/fly ash particles are mainly composed of O, Si, and metallic elements (e.g., Al, Fe, Mn, and Pb) (Figure 6i) and present single sphere or aggregation of several spheres morphology (Figures 6c and 6f). OM particles mainly contain C, O, and Si (Figure 6g). When comparing individual particles among the four sampling sites, we generally found large differences in OM particles in different stages of the NCP and the YRD.

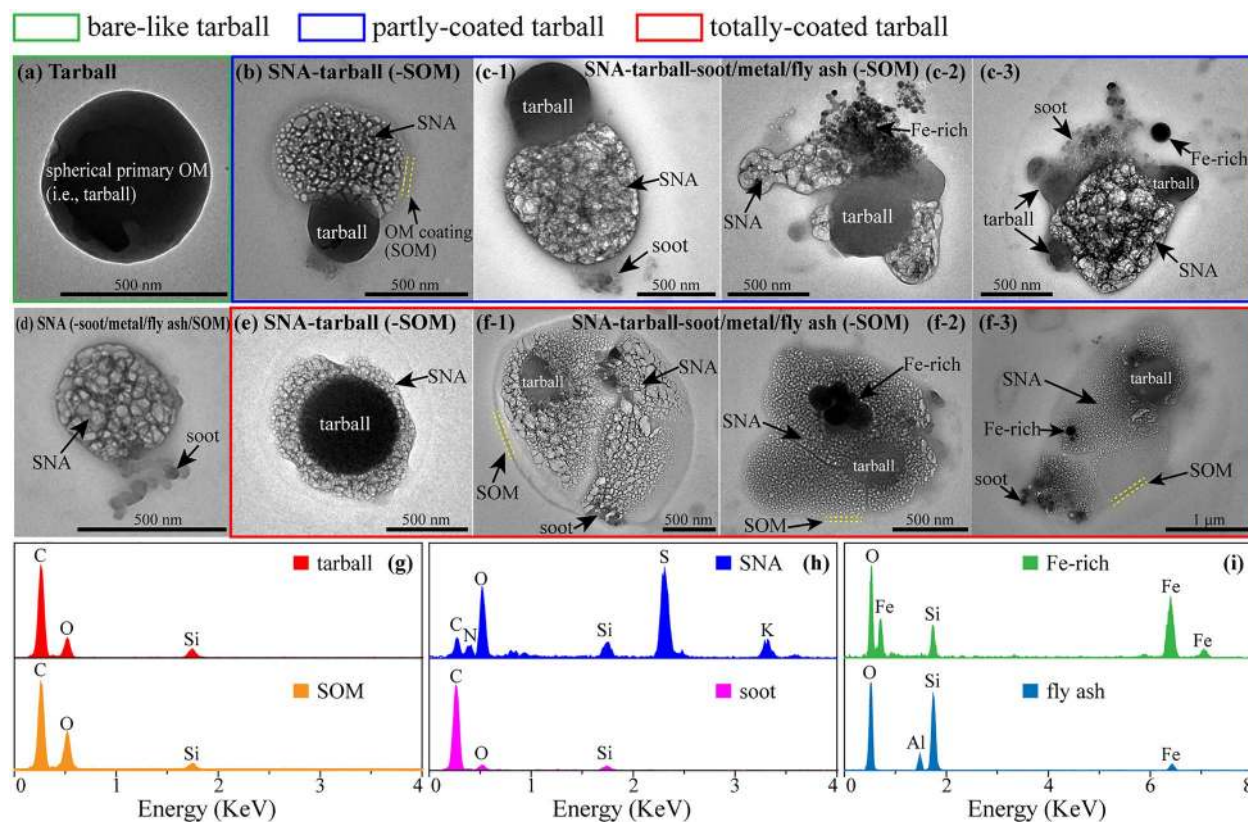


Figure 6. Typical transmission electron microscopy (TEM) images of different mixing structures of individual aerosol particles and energy-dispersive X-ray spectrometry (EDS) spectra of basic aerosol components. (a) Bare-like tarball. (b) Tarball partly coated by mixture of SNA and OM coating (SOM) particles. (c-1) Tarball partly coated by mixture of SNA, soot, and SOM particles. (c-2) Tarball partly coated by mixture of SNA and Fe-rich particles. (c-3) Tarballs partly coated by mixture of SNA, soot, and Fe-rich particles. (d) Mixture of SNA and soot particles. (e) Tarball totally coated by SNA particle. (f-1) Tarball totally coated by mixture of SNA, soot, and SOM particles. (f-2) Tarball totally coated by mixture of SNA, Fe-rich, and SOM particles. (f-3) Tarball totally coated by mixture of SNA, soot, Fe-rich, and SOM particles. (g) Tarball and SOM spectra. (h) SNA and soot spectra. (i) Fe-rich and fly ash spectra. The green, blue, and red rectangular frames represent bare-like tarball, partly coated tarball, and totally coated tarball, respectively.

In this study, OM particles mainly presented two different morphology: Spherical morphology with the average shape factor of 0.75 (Figures 6a and S5) and OM coating on SNA particles (Figures 6b and 6f). The spherical OM particles with high viscosities exist as one type of primary organic particles (Reid et al., 2018; Yuan et al., 2020) and have generally been considered to be tarballs (Adachi et al., 2019; Liu, Kong, et al., 2017; Pósfai et al., 2004; Zhang, Yuan, et al., 2018). These studies also well documented that tarballs are from combustion emissions and are good markers for household heating and cooking using biomass and coals. While OM coatings have been perceived as secondary OM (SOM) aerosols although some SOM aerosols that are homogeneously internally mixed with secondary inorganic particles could not be well identified in this study (Li, Sun, et al., 2016; Zhang, Liu, Wang, et al., 2017). That means that OM coatings are normally considered to form from the chemical transformation of VOCs in the atmosphere. Our study further semiquantified O/C ratio of individual OM particles and found lower O/C ratios of 0.15–0.16 in tarballs and a higher O/C ratio of 0.58 in SOM particles (Figure 7a). This result is consistent with O/C ratios of 0.1–0.3 in primary organic aerosols and of 0.4–1.0 in secondary organic aerosols detected by aerosol mass spectrometry in ambient air of East China (W. W. Hu et al., 2013; J. Zhao et al., 2019). Because of different energy consumption structures between the NCP and the YRD in winter, tarballs from coal burning for heating in rural households are unique in the NCP compared with the YRD with no residential coal burning for heating.

To better compare tarballs in the NCP and the YRD, we further classified the particle type based on mixing structures among four basic major particle types (Figures 6a–6f). TEM observations show that a large number of SNA particles collected in the TRT haze event in East China were internally mixed with tarballs

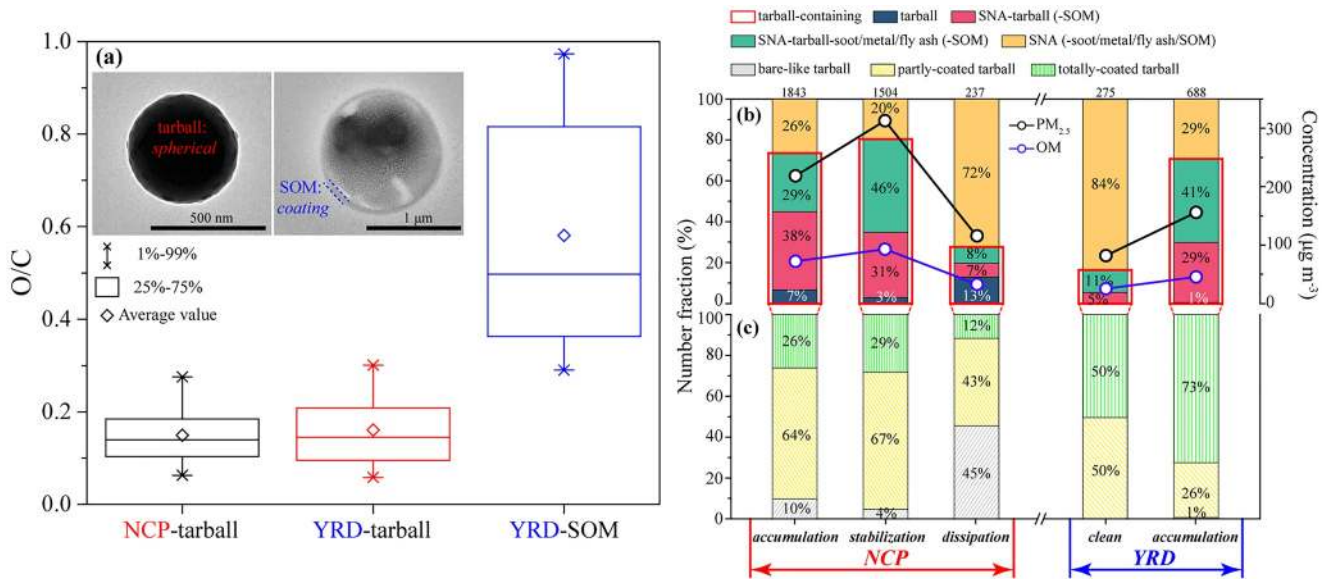


Figure 7. Ratios of O/C in OM particles and number fractions of haze particles. (a) Ratios of O/C in tarballs and SOM particles in the NCP and YRD during the TRT haze event. (b) Number fractions of haze particles combined with concentrations of PM_{2.5} and OM. (c) Number fractions of different mixing structures of tarball-containing particles. The red rectangular frames indicate tarball-containing particles. Number of analyzed particles is listed on the top of each rectangle. Number fractions of haze particles and different mixing structures of tarball-containing particles at each sampling site are showed in Figure S6.

and some were coated by SOM, which are named SNA-tarball (-SOM) particles (Figures 6b and 6e). TEM observations show that a majority of soot or metal/fly ash particles were internally mixed with tarballs and SNA particles, which are named SNA-tarball-soot/metal/fly ash (-SOM) particles (Figures 6c and 6f). To understand the variation in the number fraction and size distribution of the tarball-related particles during the TRT haze event, we regard individual particles containing tarball (i.e., externally mixed tarballs and particles with internally mixed tarballs) as tarball-containing particles (Figures 7b, 7c, and 8a–8c). If we separate tarball-containing particles in the TRT haze event, the externally mixed SNA particles and mixtures of SNA with soot, metal/fly ash, and SOM particles are together named SNA (-soot/metal/fly ash/SOM) particles (Figure 6d). Based on the mixing structures of tarball-containing particles, tarballs can be further divided into bare-like tarball (Figure 6a), partly coated tarball (i.e., tarball partly embedded in other particles) (Figures 6b and 6c), and totally coated tarball (i.e., tarball totally embedded in other particles) (Figures 6e and 6f).

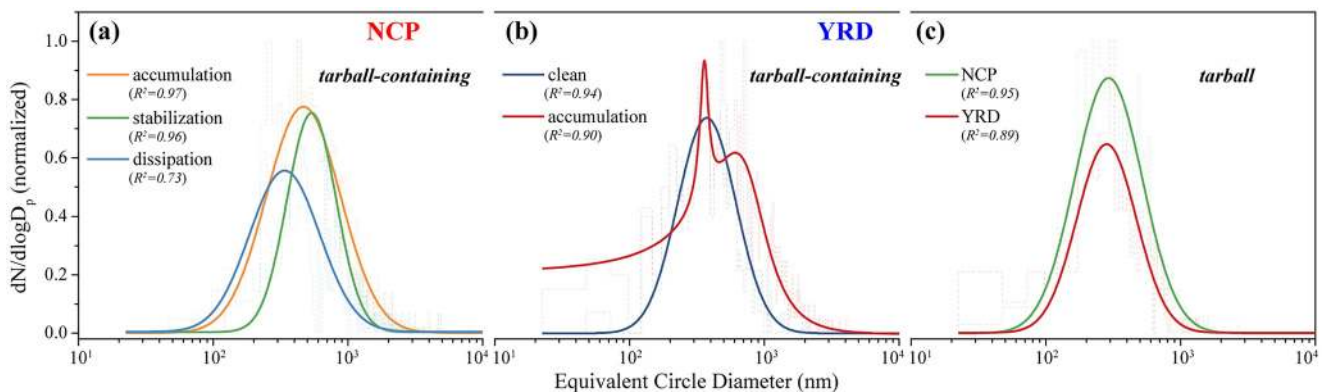


Figure 8. Size distribution of tarball-related particles during the TRT haze event from the NCP to YRD. (a–b) Tarball-containing particles. (c) Tarballs. The size distribution with single peak was fitted using lognormal distribution because lognormal distribution looks clearer. The size distribution with double peak was fitted by Lorentz distribution.

4.3. Variations of Individual Haze Particles

During the accumulation stage, the average number fraction of tarball-containing particles was 74% in the NCP based on 71% in Beijing and 75% in both Handan and Zhengzhou (Figures 7b and S6a), and their sizes mainly concentrated at 467 nm (Figure 8a). When the accumulation stage ($PM_{2.5}$: $218 \mu\text{g m}^{-3}$; OM: $72 \mu\text{g m}^{-3}$) evolved into the stabilization stage ($PM_{2.5}$: $313 \mu\text{g m}^{-3}$; OM: $93 \mu\text{g m}^{-3}$) in the NCP, the number fraction of SNA-tarball-soot/metal/fly ash (-SOM) particles largely increased from 29% to 46%, and tarball-containing and soot-containing (i.e., particles containing soot) particles slightly increased from 74% and 32% to 80% and 35% by number (Figure 7b and Table S3). The previous studies found similarly high number fractions of tarball-containing particles of 70% on light or moderate haze days in Jinan city in the NCP (S. Chen et al., 2017) and 75% during haze periods in Shenyang city in Northeast China (Zhang, Liu, Xu, et al., 2020). Moreover, we noticed that the dominant size of tarball-containing particles increased from 467 nm during the accumulation stage to 537 nm during the stabilization stage in the NCP (Figure 8a). The number fraction of individual particles including SNA aerosols (i.e., sum of SNA-tarball (-SOM), SNA-tarball-soot/metal/fly ash (-SOM), and SNA (-soot/metal/fly ash/SOM) particles) remained a high level (>90%) during the accumulation and stabilization stages in the NCP (Figure 7b). Figure 5 also shows that more SNA formed from the accumulation stage ($67 \mu\text{g m}^{-3}$) to the stabilization stage ($111 \mu\text{g m}^{-3}$) in the NCP. Consequently, bare-like tarballs decreased from 10% (by number) to 4%, but partly coated and totally coated tarballs increased from 64% and 26% to 67% and 29% (Figure 7c). These results from individual particle analysis and bulk analysis all suggest that the haze evolution promoted more tarballs aging through complex chemical reactions and/or physical coagulation.

When the stabilization stage ($PM_{2.5}$: $313 \mu\text{g m}^{-3}$; OM: $93 \mu\text{g m}^{-3}$) converted to the dissipation stage ($PM_{2.5}$: $116 \mu\text{g m}^{-3}$; OM: $33 \mu\text{g m}^{-3}$) in the NCP, the number fraction of tarball-containing particles dramatically decreased from 80% to 28% (Figure 7b). The dominant size of tarball-containing particles also decreased from 537 to 338 nm in the NCP (Figure 8a). The CWT analysis and FLEXPART model show that these haze particles in the NCP were transported into the YRD following a cold front movement (Figures 4c and 4d).

As the converse phenomenon between the YRD and the NCP during the same period, the number fraction of tarball-containing particles surprisingly increased from 16% during the clean stage to 71% during the accumulation stage in the YRD (Figure 7b). Moreover, the size distribution of tarball-containing particles in the YRD presents a second peak at 618 nm during the accumulation stage besides the first peak at 359 nm, which is close to 375 nm during the clean stage (Figure 8b). This result suggests that large numbers of tarball-containing particles with diameters of ~ 600 nm suddenly occurred in the YRD following the TRT, which is consistent with the increase of OM concentration from 25 to $45 \mu\text{g m}^{-3}$ (Figure 7b). When abundant tarball-containing particles in the NCP were transported into the YRD, we also found that the major type of tarball-containing particles changed from partly coated tarball (67% by number) in the NCP to totally coated tarball (73%) in the YRD (Figure 7c). These results provide a direct evidence that haze particles underwent complicated aging processes during the TRT, as shown in Section 4.5. Overall, the results of tarball-containing particles from individual particle analysis are coincident with OM and SNA concentrations based on the bulk measurements.

Here we isolated tarballs in all the tarball-containing particles and measured their sizes. In other words, if tarballs are internally mixed with SNA particles, we can manually measure sizes of tarball cores in TEM images. Figure 8c shows that the size distribution of tarballs in the NCP is very similar to that in the YRD during the TRT haze event, with near peaks at 281–292 nm. In addition, the O/C ratio of tarball (0.15) in the NCP is really close to that (0.16) in the YRD during the TRT haze event (Figure 7a). These comparisons show that physicochemical properties of tarballs did not change during the TRT, suggesting that tarballs are inert in the atmosphere. Therefore, we conclude that the glassy tarballs have strong physical and chemical resistance to high RH, temperature, phase change, and atmospheric oxidation.

4.4. Sources of Tarballs

Our results clearly show that over 70% of haze aerosols were tarball-containing particles in the NCP and the YRD during haze periods (Figure 7b). During winter haze days in North China, the occurrence of abundant tarballs sourced from residential heating activities have been documented well (S. Chen et al., 2017;

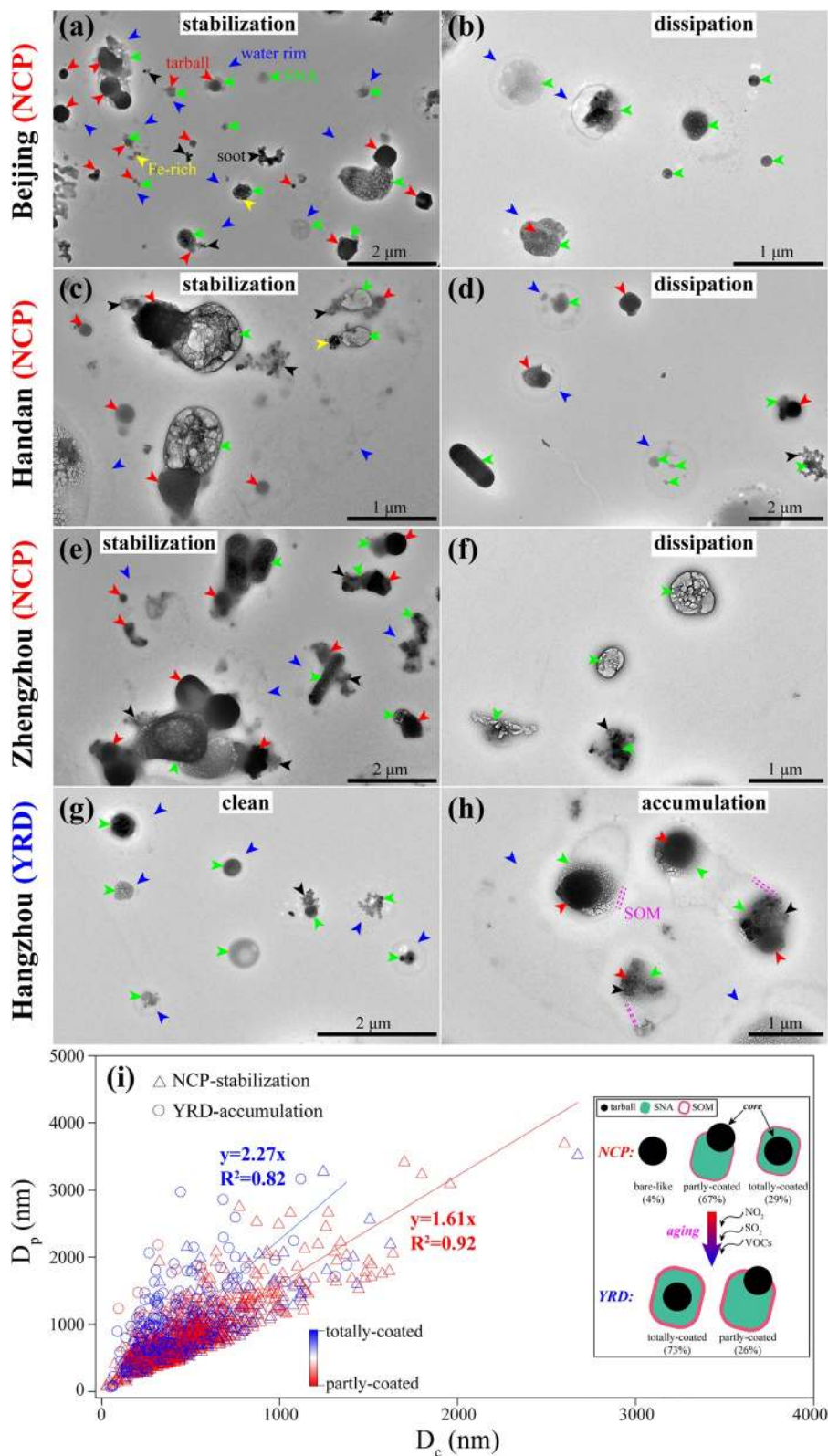
R.-J. Huang et al., 2019; J. Liu et al., 2016; Zhang, Liu, Xu, et al., 2020; J. Zhao et al., 2019). In contrast, large numbers of tarballs have not been found in South China (e.g., the YRD and the Pearl River Delta) during the non-TRT winter haze pollution due to scarce residential heating activities (R. Hu et al., 2018; Ming et al., 2017; G. Zhang et al., 2013). The previous studies have showed that C-O-Si weight ratios of tarballs can indicate their sources from coal burning and biomass burning because coal burning-derived tarballs normally contain much higher Si than biomass burning-derived tarballs (S. Chen et al., 2017; Li, Shi, et al., 2012). In this study, C-O-Si weight ratios of tarballs in the NCP and the YRD were very similar (Figure S7), suggesting that they had same source. It is well known that coal and biomass are used as the major residential solid fuels in the NCP and the YRD in winter, respectively (Yun et al., 2020). Therefore, based on the experimental analysis of tarball sources and the difference in the use of residential solid fuels between the NCP and the YRD, the sudden appearance of abundant tarballs in the YRD during the TRT haze event is strongly related to the TRT from the NCP, although local combustion emissions (e.g., biomass burning) might contribute a small proportion to tarballs (Figures 4c and 4d).

Some studies have suggested that abundant tarballs in North China in winter haze days were mainly from high-intensity residential coal burning for heating and cooking and occasional intensive biomass burning emissions (R.-J. Huang et al., 2019; J. Liu et al., 2016; Zhang, Liu, Xu, et al., 2020). High levels of K^+ and K-rich particles have always been observed, whether in the atmosphere influenced by biomass burning (Bi et al., 2011; J. Chen et al., 2017; Zhang, Liu, Xu, et al., 2020) or in the direct biomass burning emissions (Liu, Kong, et al., 2017; J. Zhai et al., 2017). Nevertheless, this work found quite low K^+ concentrations of 0.6–1.8 $\mu\text{g m}^{-3}$ and very few individual K-rich particles at the four sampling sites during the TRT haze event (S2b-e and 7b). In addition, Figure S7 clearly shows that C-O-Si weight ratios of tarballs during the TRT haze event are more similar to them from residential coal burning than biomass burning. Therefore, we rule out biomass burning as one major source of large numbers of tarballs in the NCP and the YRD. Indeed, S. Chen et al. (2017) estimated that less than 30% (by number) of tarballs were associated with biomass burning in the NCP in winter haze days. Some studies have reported that vehicle exhausts, coal-fired power plants, and industrial activities do not emit such plentiful tarballs (Li, Sun, et al., 2016), though they contribute a small proportion to primary OM in the atmosphere (Charron et al., 2019; J. Liu et al., 2016). That is the reason that individual particle analysis found abundant tarballs in North China in wintertime but not in summertime (S. Chen et al., 2017; Li, Sun, et al., 2016; Zhang, Liu, Xu, et al., 2020).

The previous studies investigated the geographical sources of haze particles in the NCP during winter (X. Li et al., 2018; J. Liu et al., 2016; P. Liu et al., 2017). They further used chemical models or aerosol measurements to reveal that local primary emissions from residential coal burning for household heating and cooking in rural villages were one major source of tarballs and continuously contributed to regional haze events in the NCP during winter (X. Li et al., 2018; J. Liu et al., 2016; P. Liu et al., 2017). Based on the CWT analysis and meteorological data during the accumulation and stabilization stages (Figures 2a–2c and 3a–3c), we knew that haze formation in Beijing was mainly influenced by anthropogenic emissions in the urban area and transported pollutants from upwind polluted Hebei province in the NCP. Haze pollution in Handan and Zhengzhou was caused by local urban and industrial emissions, as well as surrounding rural emissions. Therefore, we summarize that abundant tarballs in the NCP and the YRD during the TRT haze event were mainly directly emitted from residential coal burning in rural villages of the NCP. In addition, our TEM-EDS analysis suggests that tarballs, as inert fine aerosols, did not have any transformation, although they were internally mixed with SNA and SOM particles during the haze formation and transport (Figures 7a, 7b, and 8c). Based on the particular source, high number, and strong chemical stability of tarball, tarball identified by TEM should be considered as a particle marker to indicate the TRT haze event from the NCP to the YRD during winter.

4.5. Aging Characteristics of the TRT Haze Particles

The change in the mixing structure of aerosol particles can reflect their aging characteristics (Kandler et al., 2018; Li, Sun, et al., 2016; Moffet et al., 2013). Following the TRT, the dominant partly coated tarballs in tarball-containing haze particles in the NCP turned into the totally coated tarballs in the YRD, although tarball cores remained spherical morphology with high shape factors (Figures 7c, 9a–9h, and S5). The ratio of particle diameter (D_p) to its core diameter (D_c) is often used to quantify the aging degree of individual



aerosol particles (S. Chen et al., 2017; Moffet et al., 2013; Xu, Zhang, & Li, 2019). Figure 9i shows that the D_p/D_c ratio increased by 41% from 1.61 to 2.27 within 12 h during the TRT from the NCP to the YRD, which is much higher than 17% during the regional haze transport in the NCP reported by S. Chen et al. (2017). As a consequence, the haze particle aging during the TRT caused the dominant size of tarball-containing particles to increase from 537 to 618 nm (Figures 8a and 8b). Based on the D_p/D_c ratio and size variations of tarball-containing particles, we further obtain the average growth rates of the D_p/D_c ratio and the size of individual haze particles (100 nm–4 μm) at $\sim 5.5\% \text{ h}^{-1}$ and $\sim 6.8 \text{ nm h}^{-1}$ during the TRT from the NCP to the YRD.

It should be noted that during the TRT, the mass percentage of SNA aerosols increased from 49% in the stabilization stage in the NCP to 63% in the accumulation stage in the YRD (Figures S2a–S2e). Compared to the NCP, TEM observations show more SOM coatings on the surfaces of the TRT haze particles in the YRD (Figures 9a–9h). These results directly show that more trace reactive gases (e.g., SO_2 , NO_2 , and VOCs) participated in atmospheric aging reactions and formed thicker coatings on the surfaces of pre-existing particles during the TRT (Figure 9i). The thicker coatings also caused the significant increase in the D_p/D_c ratio during the TRT from the NCP to the YRD, compared with regional transport in the NCP (Figure 9i). Although RH under the cold front dropped from 97% to 67% in the YRD on December 30 (Figure S3a), TEM observations still show water rims around individual particles collected in the YRD. For example, Figure 9h clearly shows wet particles impacting on the substrate because each dry residual particle is surrounded by water rims. This result suggests that haze particles in the polluted air retained the wet or liquid phase during their TRT from the NCP to the YRD. Furthermore, coagulation can be significant between particles with sizes of <100 nm and >1 μm but be minor among particles of >300 nm, when the total particle number concentration is higher than 10^4 cm^{-3} (Hussein et al., 2009; Jacobson, 2002). During haze periods in the NCP, although the particle number concentration ($\sim 5 \times 10^4 \text{ cm}^{-3}$) is higher than 10^4 cm^{-3} (Guo et al., 2014), the sizes of TRT haze particles ($\sim 537 \text{ nm}$) are much larger than 300 nm (Figure 8a). This result implies that coagulation should not be dominant for particle growth during the TRT. As an alternative, heterogeneous reactions should be considered as the major pathway for the formation of SNA and SOM particles on the surfaces of pre-existing haze particles in their aging during the TRT. Overall, atmospheric aging via heterogeneous reactions during the TRT likely promoted the conversion from partly coated tarballs to totally coated tarballs and produced thick coatings on tarball-containing particles.

4.6. Hygroscopic Properties of the TRT Haze Particles

The IPH system can assess the hygroscopic properties of individual aerosol particles well (J. Sun et al., 2018). In this study, the hygroscopic growth of haze particles was obtained at the four sampling sites during the TRT haze event. Figures 10a and 10b show that the size growth of haze particles in Beijing, Zhengzhou, and Hangzhou occurs at 53%, 53%, and 43% RH, respectively, but size of haze particles in Handan starts to grow slightly at 70% RH. In general, haze particles collected in the NCP and the YRD fully deliquesce at RH of 81% and 86%, respectively (Figures 10a and 10b). We observe that the GF of haze particles has a large range of 1.05–1.22 under 90% RH in the NCP and is 1.34 in the YRD (Figure 10a). TEM observations show thicker coatings containing more SNA aerosols in the YRD compared with the NCP (Figure 9i). This result can well explain why the GF value of these TRT haze particles in the YRD is larger than them in the NCP.

It is well documented that chemical compositions of aerosol particles mainly determine their hygroscopic properties (J. Sun et al., 2018; Y. Wang et al., 2019). The lowest GF value of haze particles in Handan is related to the highest number fraction of primary particles and the lowest SNA number and mass fractions (Figures S6a and S2b–S2e) since tarball, soot, and metal/fly ash particles are hydrophobic (Li, Sun, et al., 2016; Semeniuk et al., 2007; Zhang, Yuan, et al., 2018). Meanwhile, we found that the GF values of all the TRT haze particles in the NCP and the YRD are generally much smaller than 1.4–1.8 of pure SNA particles

Figure 9. Low magnification TEM images of individual particles at the four sampling sites before and after the TRT from the NCP to YRD and variation in D_p/D_c ratio of tarball-containing particles from the NCP to YRD. (a–b) Individual particles in Beijing. (c–d) Individual particles in Handan. (e–f) Individual particles in Zhengzhou. (g–h) Individual particles in Hangzhou. (i) Scatter diagram of D_p and D_c of tarball-containing particles with different mixing structures from the NCP to YRD. Individual haze particles in panels (a, c, e, and h) were collected at 09:00 (local time), 10:00, 07:00, and 20:00 on December 30. A schematic diagram of tarball-containing particles aging during the TRT is showed in panel (i).

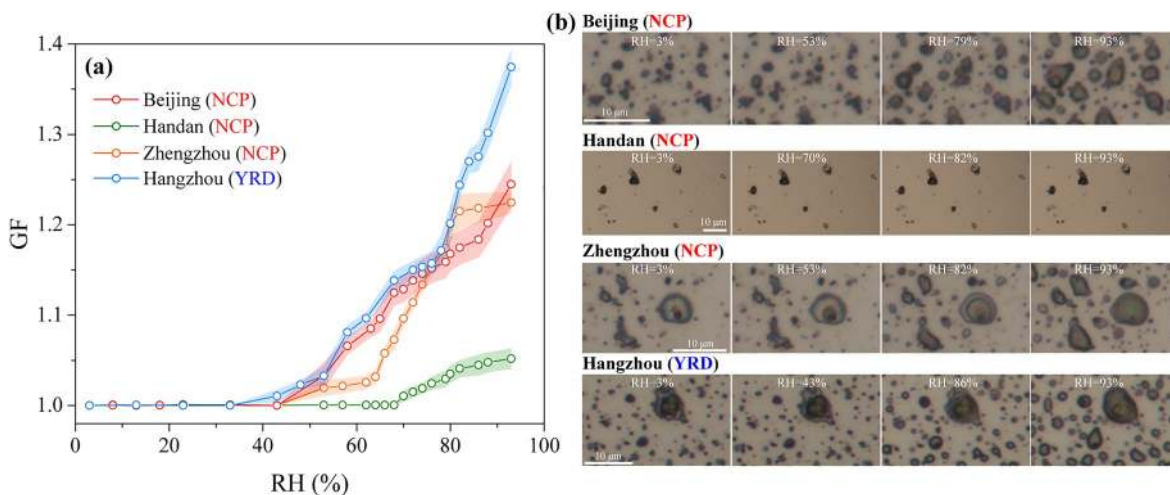


Figure 10. Hygroscopic properties of the TRT haze particles. (a) Growth factor (GF) variation of the TRT haze particles with increase of RH in Beijing, Handan, Zhengzhou, and Hangzhou. (b) Corresponding hygroscopic growth images of the TRT haze particles.

reported by J. Sun et al. (2018). This reason can be attributed to SOM and hydrophobic primary particles in individual haze particles (Figures 9a–9h) because the internally mixed SOM and hydrophobic primary particles can constrain the growth of secondary SNA particles (Chan et al., 2006; Hansen et al., 2015; Q. Liu et al., 2016; Zhang, Yuan, et al., 2018). Moreover, we noticed a higher $\text{NO}_3^-/\text{SO}_4^{2-}$ ratio and more SOM in the TRT haze particles in the YRD in contrast to those in the NCP (Figures S2b–S2e and 9a–9h). Some studies indicated that both secondary nitrates and SOM in aerosols can promote particle deliquescence at low RH (Peckhaus et al., 2012; Smith et al., 2012; J. Sun et al., 2018; Wu et al., 2011). Based on the results from bulk and individual particle analyses (Figures S2b–S2e and 9a–9i), we conclude that more nitrates and SOM in fine particles mainly result in the earlier deliquescence and larger GF value of haze particles in the YRD compared with the NCP. The hygroscopic behavior of haze particles further implies that the aged TRT haze particles, including more nitrates and SOM, can provide aqueous surfaces for the formation of secondary aerosols via heterogeneous reactions under lower RH in the YRD.

5. Atmospheric Implications

This work shows that enormous levels of haze aerosols containing tarballs (over 70% by number) from the NCP can be rapidly transported into the YRD within 12 h and further induce regional haze formation in the YRD during winter (Figures 2a–2e, 4a–4d, 5, and 7b). This is the first study proving that large numbers of tarballs emitted from residential coal burning in rural villages of the NCP can be transported thousands of kilometers and influence air quality of the YRD (Figure 11). Tarballs have been generally considered as primary brown carbon (Adachi et al., 2019; Chakrabarty et al., 2010; Sedlacek et al., 2018; Tóth et al., 2014; Zhang, Yuan, et al., 2018), which can widely absorb radiation from visible to ultraviolet wavelengths of the solar spectrum like black carbon (Hoffer et al., 2016). As a result, these abundant light-absorbing tarballs from the NCP can influence the climate in all of East China following cold fronts (Figure 11). This should be further considered in climate models.

TEM observations not only find large numbers of tarballs but also reveal that many nanosized metal particles internally mixed with SNA particles from the NCP were transported into the YRD (Figure 7b). Tarballs from residential coal burning contain plentiful carcinogenic polycyclic aromatic hydrocarbons (PAHs), and metal (e.g., Zn, Pb, Mn, and Cr) particles from heavy industries are typical toxic aerosols for human health (Y. Chen et al., 2013; Lu et al., 2020; Zhang, Schauer, et al., 2008). Our study potentially shows that the large population in the city clusters of the YRD can also be exposed to these long-range transported tarballs and metal particles during the TRT haze events (Figure 11).

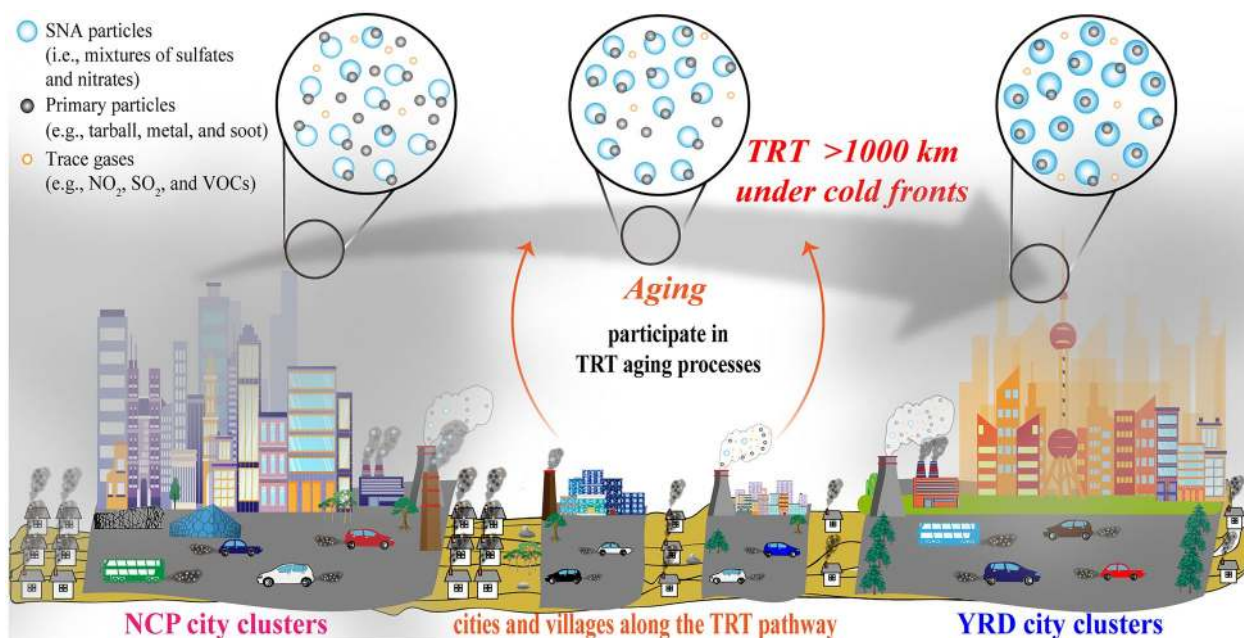


Figure 11. A schematic diagram of air pollutants TRT from city clusters in the NCP to city clusters in the YRD under cold fronts during winter. The schematic diagram shows that air pollutants such as trace gases (e.g., NO_2 , SO_2 , and VOCs) on the TRT pathway participate in the aging processes of TRT particles, promoting the conversion from partly coated tarballs to totally coated tarballs and thickening secondary coatings. The transformation of aerosol particle mixing states changes their hygroscopicity and potential optical properties. These abundant toxic and light-absorbing tarballs not only affect human health but also influence climate in all of East China.

The aging of haze particles via heterogeneous reactions in the TRT significantly transformed their mixing structures, such as tarball-containing particles changing from partly coated states in the NCP to totally coated states in the YRD (Figures 9a–9i), which is different from the short-range regional transport (S. Chen et al., 2017). The aging processes of the TRT haze particles also changed their hygroscopic properties, promoting wet surfaces of individual secondary particles at a lower RH of 43% in the YRD than 53%–70% in the NCP (Figures 10a and 10b). The variations should be important because they change these particles' optical properties and activity as potential cloud condensation nuclei (Figure 11).

Our study highlights that the influence of haze pollution is not only on the local and regional scale but is also on the trans-regional scale (Figures 1b and 11). This work shows for the first time that the TRT haze events can carry large numbers of nanosized primary particles (e.g., tarball, metal, fly ash, soot, and mineral) from the NCP to the YRD in addition to trace gases (e.g., SO_2 , NO_x , and VOCs) and SNA aerosols reported by Li, Wang, et al. (2019). Therefore, long-range transport of nanosized primary particles in the global atmosphere should receive more attention because they have large potential impacts on climate and human health.

By understanding the chemical compositions, aging, and hygroscopicity of aerosol particles during a TRT haze event, we can find that regional air pollution is not limited by administrative regions or national boundaries. Topographical features and large-scale meteorological characteristics need to be considered because they influence the formation of the TRT events. In addition, international trade among different countries or regions can cause the potential TRT of air pollutants (Lin et al., 2014; Q. Zhang et al., 2017). Consequently, emission controls in only one region are insufficient, and the joint control among multiple regions is crucial to reduce the level of air pollution.

In summary, TRT and TRT-related transformation of air pollutants should receive more attention because of their trans-regional and global impacts on human health, climate, and ecology (X. Huang et al., 2020). This can provide important information for producing simulations of climate changes and health effects.

Data Availability Statement

All observed and experimental data are available on figshare at <https://doi.org/10.6084/m9.figshare.13490751.v1>.

Acknowledgments

This work was funded by the National Natural Science Foundation of China (42075096, 91844301, and 41807305), the National Key R&D Program of China (2017YFC0212700), and Zhejiang Provincial Natural Science Foundation of China (LZ19D050001).

References

- Adachi, K., Sedlacek, A. J., Kleinman, L., Springston, S. R., Wang, J., Chand, D., et al. (2019). Spherical tarball particles form through rapid chemical and physical changes of organic matter in biomass-burning smoke. *Proceedings of the National Academy of Sciences*, *116*(39), 19336–19341. <https://doi.org/10.1073/pnas.1900129116>
- Bi, X., Zhang, G., Li, L., Wang, X., Li, M., Sheng, G., et al. (2011). Mixing state of biomass burning particles by single particle aerosol mass spectrometer in the urban area of PRD, China. *Atmospheric Environment*, *45*(20), 3447–3453. <https://doi.org/10.1016/j.atmosenv.2011.03.034>
- Chakrabarty, R. K., Moosmüller, H., Chen, L.-W. A., Lewis, K., Arnott, W. P., Mazzoleni, C., et al. (2010). Brown carbon in tar balls from smoldering biomass combustion. *Atmospheric Chemistry and Physics*, *10*(13), 6363–6370. <https://doi.org/10.5194/acp-10-6363-2010>
- Chan, M. N., Lee, A. K. Y., & Chan, C. K. (2006). Responses of ammonium sulfate particles coated with glutaric acid to cyclic changes in relative humidity: Hygroscopicity and Raman characterization. *Environmental Science & Technology*, *40*(22), 6983–6989. <https://doi.org/10.1021/es060928c>
- Charron, A., Polo-Rehn, L., Besombes, J.-L., Golly, B., Buisson, C., Chanut, H., et al. (2019). Identification and quantification of particulate tracers of exhaust and non-exhaust vehicle emissions. *Atmospheric Chemistry and Physics*, *19*(7), 5187–5207. <https://doi.org/10.5194/acp-19-5187-2019>
- Chen, J., Li, C., Ristovski, Z., Milic, A., Gu, Y., Islam, M. S., et al. (2017a). A review of biomass burning: Emissions and impacts on air quality, health and climate in China. *Science of the Total Environment*, *579*, 1000–1034. <https://doi.org/10.1016/j.scitotenv.2016.11.025>
- Chen, S., Xu, L., Zhang, Y., Chen, B., Wang, X., Zhang, X., et al. (2017b). Direct observations of organic aerosols in common wintertime hazes in North China: Insights into direct emissions from Chinese residential stoves. *Atmospheric Chemistry and Physics*, *17*(2), 1259–1270. <https://doi.org/10.5194/acp-17-1259-2017>
- Chen, Y., Ebenstein, A., Greenstone, M., & Li, H. (2013). Evidence on the impact of sustained exposure to air pollution on life expectancy from China's Huai River policy. *Proceedings of the National Academy of Sciences*, *110*(32), 12936–12941. <https://doi.org/10.1073/pnas.1300018110>
- Cheng, Z., Wang, S., Jiang, J., Fu, Q., Chen, C., Xu, B., et al. (2013). Long-term trend of haze pollution and impact of particulate matter in the Yangtze River Delta, China. *Environmental Pollution*, *182*, 101–110. <https://doi.org/10.1016/j.envpol.2013.06.043>
- Chi, J. W., Li, W. J., Zhang, D. Z., Zhang, J. C., Lin, Y. T., Shen, X. J., et al. (2015). Sea salt aerosols as a reactive surface for inorganic and organic acidic gases in the Arctic troposphere. *Atmospheric Chemistry and Physics*, *15*(19), 11341–11353. <https://doi.org/10.5194/acp-15-11341-2015>
- Conway, T. M., Hamilton, D. S., Shelley, R. U., Aguilar-Islas, A. M., Landing, W. M., Mahowald, N. M., & John, S. G. (2019). Tracing and constraining anthropogenic aerosol iron fluxes to the North Atlantic Ocean using iron isotopes. *Nature Communications*, *10*, 2628. <https://doi.org/10.1038/s41467-019-10457-w>
- Eckhardt, S., Breivik, K., Li, Y. F., Manø, S., & Stohl, A. (2009). Source regions of some persistent organic pollutants measured in the atmosphere at Birkenes, Norway. *Atmospheric Chemistry and Physics*, *9*(17), 6597–6610. <https://doi.org/10.5194/acp-9-6597-2009>
- Ge, B., Wang, Z., Lin, W., Xu, X., Li, J., Ji, D., & Ma, Z. (2018). Air pollution over the North China Plain and its implication of regional transport: A new sight from the observed evidences. *Environmental Pollution*, *234*, 29–38. <https://doi.org/10.1016/j.envpol.2017.10.084>
- Guo, S., Hu, M., Zamora, M. L., Peng, J., Shang, D., Zheng, J., et al. (2014). Elucidating severe urban haze formation in China. *Proceedings of the National Academy of Sciences*, *111*(49), 17373–17378. <https://doi.org/10.1073/pnas.1419604111>
- Hansen, A. M. K., Hong, J., Raatikainen, T., Kristensen, K., Ylisirniö, A., Virtanen, A., et al. (2015). Hygroscopic properties and cloud condensation nuclei activation of limonene-derived organosulfates and their mixtures with ammonium sulfate. *Atmospheric Chemistry and Physics*, *15*(24), 14071–14089. <https://doi.org/10.5194/acp-15-14071-2015>
- He, J., Gong, S., Zhou, C., Lu, S., Wu, L., Chen, Y., et al. (2018). Analyses of winter circulation types and their impacts on haze pollution in Beijing. *Atmospheric Environment*, *192*, 94–103. <https://doi.org/10.1016/j.atmosenv.2018.08.060>
- Herrmann, E., Ding, A. J., Kerminen, V.-M., Petäjä, T., Yang, X. Q., Sun, J. N., et al. (2014). Aerosols and nucleation in eastern China: First insights from the new SORPES-NJU station. *Atmospheric Chemistry and Physics*, *14*(4), 2169–2183. <https://doi.org/10.5194/acp-14-2169-2014>
- Hoffer, A., Tóth, A., Nyíró-Kósa, I., Pósfai, M., & Gelencsér, A. (2016). Light absorption properties of laboratory-generated tar ball particles. *Atmospheric Chemistry and Physics*, *16*(1), 239–246. <https://doi.org/10.5194/acp-16-239-2016>
- Hou, X., Zhu, B., Kumar, K. R., de Leeuw, G., Lu, W., Huang, Q., & Zhu, X. (2020). Establishment of conceptual schemas of surface synoptic meteorological situations affecting fine particulate pollution across eastern China in the winter. *Journal of Geophysical Research: Atmospheres*, *125*(23), e2020JD033153. <https://doi.org/10.1029/2020JD033153>
- Hu, R., Wang, H., Yin, Y., Chen, K., Zhu, B., Zhang, Z., et al. (2018). Mixing state of ambient aerosols during different fog-haze pollution episodes in the Yangtze River Delta, China. *Atmospheric Environment*, *178*, 1–10. <https://doi.org/10.1016/j.atmosenv.2018.01.032>
- Hu, W. W., Hu, M., Yuan, B., Jimenez, J. L., Tang, Q., Peng, J. F., et al. (2013). Insights on organic aerosol aging and the influence of coal combustion at a regional receptor site of central eastern China. *Atmospheric Chemistry and Physics*, *13*(19), 10095–10112. <https://doi.org/10.5194/acp-13-10095-2013>
- Huang, R.-J., Wang, Y., Cao, J., Lin, C., Duan, J., Chen, Q., et al. (2019). Primary emissions versus secondary formation of fine particulate matter in the most polluted city (Shijiazhuang) in North China. *Atmospheric Chemistry and Physics*, *19*(4), 2283–2298. <https://doi.org/10.5194/acp-19-2283-2019>
- Huang, X., Ding, A., Wang, Z., Ding, K., Gao, J., Chai, F., & Fu, C. (2020). Amplified transboundary transport of haze by aerosol-boundary layer interaction in China. *Nature Geoscience*, *13*(6), 428–434. <https://doi.org/10.1038/s41561-020-0583-4>
- Hussein, T., Hruška, A., Dohányosová, P., Džumbová, L., Hemerka, J., Kulmala, M., & Smolík, J. (2009). Deposition rates on smooth surfaces and coagulation of aerosol particles inside a test chamber. *Atmospheric Environment*, *43*(4), 905–914. <https://doi.org/10.1016/j.atmosenv.2008.10.059>

- Jacobson, M. Z. (2002). Analysis of aerosol interactions with numerical techniques for solving coagulation, nucleation, condensation, dissolution, and reversible chemistry among multiple size distributions. *Journal of Geophysical Research*, *107*(D19), AAC 2-1–AAC 2-23. <https://doi.org/10.1029/2001JD002044>
- Kandler, K., Schneiders, K., Ebert, M., Hartmann, M., Weinbruch, S., Prass, M., & Pöhlker, C. (2018). Composition and mixing state of atmospheric aerosols determined by electron microscopy: Method development and application to aged Saharan dust deposition in the Caribbean boundary layer. *Atmospheric Chemistry and Physics*, *18*(18), 13429–13455. <https://doi.org/10.5194/acp-18-13429-2018>
- Kang, H., Zhu, B., Gao, J., He, Y., Wang, H., Su, J., et al. (2019). Potential impacts of cold frontal passage on air quality over the Yangtze River Delta, China. *Atmospheric Chemistry and Physics*, *19*(6), 3673–3685. <https://doi.org/10.5194/acp-19-3673-2019>
- Lelieveld, J., Pozzer, A., Poschl, U., Fnais, M., Haines, A., & Munzel, T. (2020). Loss of life expectancy from air pollution compared to other risk factors: A worldwide perspective. *Cardiovascular Research*, *116*(11), 1910–1917. <https://doi.org/10.1093/cvr/cvaa025>
- Li, J., Liao, H., Hu, J., & Li, N. (2019a). Severe particulate pollution days in China during 2013–2018 and the associated typical weather patterns in Beijing-Tianjin-Hebei and the Yangtze River Delta regions. *Environmental Pollution*, *248*, 74–81. <https://doi.org/10.1016/j.envpol.2019.01.124>
- Li, M., Huang, X., Zhu, L., Li, J., Song, Y., Cai, X., & Xie, S. (2012a). Analysis of the transport pathways and potential sources of PM₁₀ in Shanghai based on three methods. *Science of the Total Environment*, *414*, 525–534. <https://doi.org/10.1016/j.scitotenv.2011.10.054>
- Li, M., Wang, T., Xie, M., Li, S., Zhuang, B., Huang, X., et al. (2019b). Formation and evolution mechanisms for two extreme haze episodes in the Yangtze River Delta region of China during winter 2016. *Journal of Geophysical Research: Atmospheres*, *124*, 3607–3623. <https://doi.org/10.1029/2019JD030535>
- Li, W., Shi, Z., Zhang, D., Zhang, X., Li, P., Feng, Q., et al. (2012b). Haze particles over a coal-burning region in the China Loess Plateau in winter: Three flight missions in December 2010. *Journal of Geophysical Research: Atmospheres*, *117*(D12). <https://doi.org/10.1029/2012JD017720>
- Li, W., Sun, J., Xu, L., Shi, Z., Riemer, N., Sun, Y., et al. (2016). A conceptual framework for mixing structures in individual aerosol particles. *Journal of Geophysical Research: Atmospheres*, *121*(22), 13784–13798. <https://doi.org/10.1002/2016JD025252>
- Li, W., Xu, L., Liu, X., Zhang, J., Lin, Y., Yao, X., et al. (2017a). Air pollution–aerosol interactions produce more bioavailable iron for ocean ecosystems. *Science Advances*, *3*(3), e1601749. <https://doi.org/10.1126/sciadv.1601749>
- Li, X., Wu, J., Elser, M., Feng, T., Cao, J., El-Haddad, I., et al. (2018). Contributions of residential coal combustion to the air quality in Beijing-Tianjin-Hebei (BTH), China: A case study. *Atmospheric Chemistry and Physics*, *18*(14), 10675–10691. <https://doi.org/10.5194/acp-18-10675-2018>
- Li, Y. J., Lee, B. P., Su, L., Fung, J. C. H., & Chan, C. K. (2015). Seasonal characteristics of fine particulate matter (PM) based on high-resolution time-of-flight aerosol mass spectrometric (HR-ToF-AMS) measurements at the HKUST Supersite in Hong Kong. *Atmospheric Chemistry and Physics*, *15*(1), 37–53. <https://doi.org/10.5194/acp-15-37-2015>
- Li, Z., Guo, J., Ding, A., Liao, H., Liu, J., Sun, Y., et al. (2017b). Aerosol and boundary-layer interactions and impact on air quality. *National Science Review*, *4*(6), 810–833. <https://doi.org/10.1093/nsr/nwx117>
- Lin, J., Pan, D., Davis, S. J., Zhang, Q., He, K., Wang, C., et al. (2014). China's international trade and air pollution in the United States. *Proceedings of the National Academy of Sciences*, *111*(5), 1736–1741. <https://doi.org/10.1073/pnas.1312860111>
- Liu, C., Ma, Z., Mu, Y., Liu, J., Zhang, C., Zhang, Y., et al. (2017a). The levels, variation characteristics, and sources of atmospheric non-methane hydrocarbon compounds during wintertime in Beijing, China. *Atmospheric Chemistry and Physics*, *17*(17), 10633–10649. <https://doi.org/10.5194/acp-17-10633-2017>
- Liu, J., Mauzerall, D. L., Chen, Q., Zhang, Q., Song, Y., Peng, W., et al. (2016a). Air pollutant emissions from Chinese households: A major and underappreciated ambient pollution source. *Proceedings of the National Academy of Sciences*, *113*(28), 7756–7761. <https://doi.org/10.1073/pnas.1604537113>
- Liu, L., Kong, S., Zhang, Y., Wang, Y., Xu, L., Yan, Q., et al. (2017b). Morphology, composition, and mixing state of primary particles from combustion sources—crop residue, wood, and solid waste. *Scientific Reports*, *7*, 5047. <https://doi.org/10.1038/s41598-017-05357-2>
- Liu, L., Zhang, J., Du, R., Teng, X., Hu, R., Yuan, Q., et al. (2020). Chemistry of atmospheric fine particles during the COVID-19 pandemic in a megacity of eastern China. *Geophysical Research Letters*, *48*(2), e2020GL091611. <https://doi.org/10.1029/2020GL091611>
- Liu, P., Zhang, C., Xue, C., Mu, Y., Liu, J., Zhang, Y., et al. (2017c). The contribution of residential coal combustion to atmospheric PM_{2.5} in northern China during winter. *Atmospheric Chemistry and Physics*, *17*(18), 11503–11520. <https://doi.org/10.5194/acp-17-11503-2017>
- Liu, Q., Jing, B., Peng, C., Tong, S., Wang, W., & Ge, M. (2016b). Hygroscopicity of internally mixed multi-component aerosol particles of atmospheric relevance. *Atmospheric Environment*, *125*, 69–77. <https://doi.org/10.1016/j.atmosenv.2015.11.003>
- Liu, S., Hua, S., Wang, K., Qiu, P., Liu, H., Wu, B., et al. (2018). Spatial-temporal variation characteristics of air pollution in Henan of China: Localized emission inventory, WRF/Chem simulations and potential source contribution analysis. *Science of the Total Environment*, *624*, 396–406. <https://doi.org/10.1016/j.scitotenv.2017.12.102>
- Lu, D., Luo, Q., Chen, R., Zhuansun, Y., Jiang, J., Wang, W., et al. (2020). Chemical multi-fingerprinting of exogenous ultrafine particles in human serum and pleural effusion. *Nature Communications*, *11*(1), 2567. <https://doi.org/10.1038/s41467-020-16427-x>
- Lyu, R., Shi, Z., Alam, M. S., Wu, X., Liu, D., Vu, T. V., et al. (2019). Insight into the composition of organic compounds ($\geq C_6$) in PM_{2.5} in wintertime in Beijing, China. *Atmospheric Chemistry and Physics*, *19*(16), 10865–10881. <https://doi.org/10.5194/acp-19-10865-2019>
- Ming, L., Jin, L., Li, J., Fu, P., Yang, W., Liu, D., et al. (2017). PM_{2.5} in the Yangtze River Delta, China: Chemical compositions, seasonal variations, and regional pollution events. *Environmental Pollution*, *223*, 200–212. <https://doi.org/10.1016/j.envpol.2017.01.013>
- Moffet, R. C., Rödel, T. C., Kelly, S. T., Yu, X. Y., Carroll, G. T., Fast, J., et al. (2013). Spectro-microscopic measurements of carbonaceous aerosol aging in Central California. *Atmospheric Chemistry and Physics*, *13*(20), 10445–10459. <https://doi.org/10.5194/acp-13-10445-2013>
- Pan, X., Ge, B., Wang, Z., Tian, Y., Liu, H., Wei, L., et al. (2019). Synergistic effect of water-soluble species and relative humidity on morphological changes in aerosol particles in the Beijing megacity during severe pollution episodes. *Atmospheric Chemistry and Physics*, *19*(1), 219–232. <https://doi.org/10.5194/acp-19-219-2019>
- Pan, Y., Wang, Y., Sun, Y., Tian, S., & Cheng, M. (2013). Size-resolved aerosol trace elements at a rural mountainous site in Northern China: Importance of regional transport. *Science of the Total Environment*, *461–462*, 761–771. <https://doi.org/10.1016/j.scitotenv.2013.04.065>
- Peckhaus, A., Grass, S., Treuel, L., & Zellner, R. (2012). Deliquescence and efflorescence behavior of ternary inorganic/organic/water aerosol particles. *The Journal of Physical Chemistry A*, *116*(24), 6199–6210. <https://doi.org/10.1021/jp211522t>
- Petit, J.-E., Favez, O., Albinet, A., & Canonaco, F. (2017). A user-friendly tool for comprehensive evaluation of the geographical origins of atmospheric pollution: Wind and trajectory analyses. *Environmental Modelling & Software*, *88*, 183–187. <https://doi.org/10.1016/j.envsoft.2016.11.022>
- Pósfai, M., Gelencsér, A., Simonics, R., Arató, K., Li, J., Hobbs, P. V., & Buseck, P. R. (2004). Atmospheric tar balls: Particles from biomass and biofuel burning. *Journal of Geophysical Research*, *109*(D6), D06213. <https://doi.org/10.1029/2003JD004169>

- Reid, J. P., Bertram, A. K., Topping, D. O., Laskin, A., Martin, S. T., Petters, M. D., et al. (2018). The viscosity of atmospherically relevant organic particles. *Nature Communications*, 9, 956. <https://doi.org/10.1038/s41467-018-03027-z>
- Sedlacek, A. J., III, Buseck, P. R., Adachi, K., Onasch, T. B., Springston, S. R., & Kleinman, L. (2018). Formation and evolution of tar balls from northwestern US wildfires. *Atmospheric Chemistry and Physics*, 18(15), 11289–11301. <https://doi.org/10.5194/acp-18-11289-2018>
- Semeniuk, T. A., Wise, M. E., Martin, S. T., Russell, L. M., & Buseck, P. R. (2007). Hygroscopic behavior of aerosol particles from biomass fires using environmental transmission electron microscopy. *Journal of Atmospheric Chemistry*, 56(3), 259–273. <https://doi.org/10.1007/s10874-006-9055-5>
- Shao, J., Chen, Q., Wang, Y., Lu, X., He, P., Sun, Y., et al. (2019). Heterogeneous sulfate aerosol formation mechanisms during wintertime Chinese haze events: Air quality model assessment using observations of sulfate oxygen isotopes in Beijing. *Atmospheric Chemistry and Physics*, 19(9), 6107–6123. <https://doi.org/10.5194/acp-19-6107-2019>
- Shi, C., Nduka, I. C., Yang, Y., Huang, Y., Yao, R., Zhang, H., et al. (2020). Characteristics and meteorological mechanisms of transboundary air pollution in a persistent heavy PM_{2.5} pollution episode in Central-East China. *Atmospheric Environment*, 223, 117239. <https://doi.org/10.1016/j.atmosenv.2019.117239>
- Shrivastava, M., Lou, S., Zelenyuk, A., Easter, R. C., Corley, R. A., Thrall, B. D., et al. (2017). Global long-range transport and lung cancer risk from polycyclic aromatic hydrocarbons shielded by coatings of organic aerosol. *Proceedings of the National Academy of Sciences*, 114(6), 1246–1251. <https://doi.org/10.1073/pnas.1618475114>
- Shu, L., Xie, M., Gao, D., Wang, T., Fang, D., Liu, Q., et al. (2017). Regional severe particle pollution and its association with synoptic weather patterns in the Yangtze River Delta region, China. *Atmospheric Chemistry and Physics*, 17(21), 12871–12891. <https://doi.org/10.5194/acp-17-12871-2017>
- Smith, M. L., Bertram, A. K., & Martin, S. T. (2012). Deliquescence, efflorescence, and phase miscibility of mixed particles of ammonium sulfate and isoprene-derived secondary organic material. *Atmospheric Chemistry and Physics*, 12(20), 9613–9628. <https://doi.org/10.5194/acp-12-9613-2012>
- Stohl, A., Forster, C., Frank, A., Seibert, P., & Wotawa, G. (2005). Technical note: The Lagrangian particle dispersion model FLEXPART version 6.2. *Atmospheric Chemistry and Physics*, 5(9), 2461–2474. <https://doi.org/10.5194/acp-5-2461-2005>
- Sun, J., Liu, L., Xu, L., Wang, Y., Wu, Z., Hu, M., et al. (2018a). Key role of nitrate in phase transitions of urban particles: Implications of important reactive surfaces for secondary aerosol formation. *Journal of Geophysical Research: Atmospheres*, 123(2), 1234–1243. <https://doi.org/10.1002/2017JD027264>
- Sun, T., Che, H., Qi, B., Wang, Y., Dong, Y., Xia, X., et al. (2018b). Aerosol optical characteristics and their vertical distributions under enhanced haze pollution events: Effect of the regional transport of different aerosol types over eastern China. *Atmospheric Chemistry and Physics*, 18(4), 2949–2971. <https://doi.org/10.5194/acp-18-2949-2018>
- Suzuki, K., & Takemura, T. (2019). Perturbations to global energy budget due to absorbing and scattering aerosols. *Journal of Geophysical Research: Atmospheres*, 124(4), 2194–2209. <https://doi.org/10.1029/2018jd029808>
- Tóth, A., Hoffer, A., Nyíró-Kósa, I., Pósfai, M., & Gelencsér, A. (2014). Atmospheric tar balls: Aged primary droplets from biomass burning? *Atmospheric Chemistry and Physics*, 14(13), 6669–6675. <https://doi.org/10.5194/acp-14-6669-2014>
- Wang, F., Chen, Y., Meng, X., Fu, J., & Wang, B. (2016a). The contribution of anthropogenic sources to the aerosols over East China Sea. *Atmospheric Environment*, 127, 22–33. <https://doi.org/10.1016/j.atmosenv.2015.12.002>
- Wang, G., Zhang, R., Gomez, M. E., Yang, L., Levy Zamora, M., Hu, M., et al. (2016b). Persistent sulfate formation from London Fog to Chinese haze. *Proceedings of the National Academy of Sciences*, 113(48), 13630–13635. <https://doi.org/10.1073/pnas.1616540113>
- Wang, H., An, J., Shen, L., Zhu, B., Pan, C., Liu, Z., et al. (2014). Mechanism for the formation and microphysical characteristics of sub-micron aerosol during heavy haze pollution episode in the Yangtze River Delta, China. *Science of the Total Environment*, 490, 501–508. <https://doi.org/10.1016/j.scitotenv.2014.05.009>
- Wang, H., Shi, G. Y., Zhang, X. Y., Gong, S. L., Tan, S. C., Chen, B., et al. (2015). Mesoscale modelling study of the interactions between aerosols and PBL meteorology during a haze episode in China Jing-Jin-Ji and its near surrounding region – Part 2: Aerosols' radiative feedback effects. *Atmospheric Chemistry and Physics*, 15(6), 3277–3287. <https://doi.org/10.5194/acp-15-3277-2015>
- Wang, J., Li, J., Ye, J., Zhao, J., Wu, Y., Hu, J., et al. (2020). Fast sulfate formation from oxidation of SO₂ by NO₂ and HONO observed in Beijing haze. *Nature Communications*, 11, 2844. <https://doi.org/10.1038/s41467-020-16683-x>
- Wang, Y., Li, Z., Zhang, R., Jin, X., Xu, W., Fan, X., et al. (2019). Distinct ultrafine- and accumulation-mode particle properties in clean and polluted urban environments. *Geophysical Research Letters*, 46(19), 10918–10925. <https://doi.org/10.1029/2019gl084047>
- Wu, Z. J., Nowak, A., Poulain, L., Herrmann, H., & Wiedensohler, A. (2011). Hygroscopic behavior of atmospherically relevant water-soluble carboxylic salts and their influence on the water uptake of ammonium sulfate. *Atmospheric Chemistry and Physics*, 11(24), 12617–12626. <https://doi.org/10.5194/acp-11-12617-2011>
- Xing, L., Fu, T.-M., Cao, J. J., Lee, S. C., Wang, G. H., Ho, K. F., et al. (2013). Seasonal and spatial variability of the OM/OC mass ratios and high regional correlation between oxalic acid and zinc in Chinese urban organic aerosols. *Atmospheric Chemistry and Physics*, 13(8), 4307–4318. <https://doi.org/10.5194/acp-13-4307-2013>
- Xu, L., Fukushima, S., Sobanska, S., Murata, K., Naganuma, A., Liu, L., et al. (2020a). Tracing the evolution of morphology and mixing state of soot particles along with the movement of an Asian dust storm. *Atmospheric Chemistry and Physics*, 20(22), 14321–14332. <https://doi.org/10.5194/acp-20-14321-2020>
- Xu, L., Zhang, D., & Li, W. (2019). Microscopic comparison of aerosol particles collected at an urban site in North China and a coastal site in Japan. *Science of the Total Environment*, 669, 948–954. <https://doi.org/10.1016/j.scitotenv.2019.03.163>
- Xu, L., Zhang, J., Sun, X., Xu, S., Shan, M., Yuan, Q., et al. (2020b). Variation in concentration and sources of black carbon in a megacity of China during the COVID-19 pandemic. *Geophysical Research Letters*, 47(23), e2020GL090444. <https://doi.org/10.1029/2020GL090444>
- Xue, J., Yu, X., Yuan, Z., Griffith, S. M., Lau, A. K. H., Seinfeld, J. H., & Yu, J. Z. (2019). Efficient control of atmospheric sulfate production based on three formation regimes. *Nature Geoscience*, 12(12), 977–982. <https://doi.org/10.1038/s41561-019-0485-5>
- Yang, S., Ma, Y. L., Duan, F. K., He, K. B., Wang, L. T., Wei, Z., et al. (2018). Characteristics and formation of typical winter haze in Handan, one of the most polluted cities in China. *Science of the Total Environment*, 613–614, 1367–1375. <https://doi.org/10.1016/j.scitotenv.2017.08.033>
- Yao, L., Garmash, O., Bianchi, F., Zheng, J., Yan, C., Kontkanen, J., et al. (2018). Atmospheric new particle formation from sulfuric acid and amines in a Chinese megacity. *Science*, 361(6399), 278–281. <https://doi.org/10.1126/science.aao4839>
- Yuan, Q., Xu, J., Liu, L., Zhang, A., Liu, Y., Zhang, J., et al. (2020). Evidence for Large Amounts of Brown Carbonaceous Tarballs in the Himalayan Atmosphere. *Environmental Science & Technology Letters*, 8(1), 16–23. <https://doi.org/10.1021/acs.estlett.0c00735>
- Yue, S., Bikkina, S., Gao, M., Barrie, L. A., Kawamura, K., & Fu, P. (2019). Sources and radiative absorption of water-soluble brown carbon in the high Arctic atmosphere. *Geophysical Research Letters*, 46(24), 14881–14891. <https://doi.org/10.1029/2019gl085318>

- Yun, X., Shen, G., Shen, H., Meng, W., Chen, Y., Xu, H., et al. (2020). Residential solid fuel emissions contribute significantly to air pollution and associated health impacts in China. *Science Advances*, 6(44), eaba7621. <https://doi.org/10.1126/sciadv.aba7621>
- Zhai, J., Lu, X., Li, L., Zhang, Q., Zhang, C., Chen, H., et al. (2017). Size-resolved chemical composition, effective density, and optical properties of biomass burning particles. *Atmospheric Chemistry and Physics*, 17(12), 7481–7493. <https://doi.org/10.5194/acp-17-7481-2017>
- Zhai, S., An, X., Zhao, T., Sun, Z., Wang, W., Hou, Q., et al. (2018). Detection of critical PM_{2.5} emission sources and their contributions to a heavy haze episode in Beijing, China, using an adjoint model. *Atmospheric Chemistry and Physics*, 18(9), 6241–6258. <https://doi.org/10.5194/acp-18-6241-2018>
- Zhang, F., Wang, Y., Peng, J., Chen, L., Sun, Y., Duan, L., et al. (2020a). An unexpected catalyst dominates formation and radiative forcing of regional haze. *Proceedings of the National Academy of Sciences*, 117(8), 3960–3966. <https://doi.org/10.1073/pnas.1919343117>
- Zhang, G., Bi, X., Chan, L. Y., Wang, X., Sheng, G., & Fu, J. (2013). Size-segregated chemical characteristics of aerosol during haze in an urban area of the Pearl River Delta region, China. *Urban Climate*, 4, 74–84. <https://doi.org/10.1016/j.uclim.2013.05.002>
- Zhang, J., Liu, L., Wang, Y., Ren, Y., Wang, X., Shi, Z., et al. (2017a). Chemical composition, source, and process of urban aerosols during winter haze formation in Northeast China. *Environmental Pollution*, 231, 357–366. <https://doi.org/10.1016/j.envpol.2017.07.102>
- Zhang, J., Liu, L., Xu, L., Lin, Q., Zhao, H., Wang, Z., et al. (2020b). Exploring wintertime regional haze in northeast China: Role of coal and biomass burning. *Atmospheric Chemistry and Physics*, 20(9), 5355–5372. <https://doi.org/10.5194/acp-20-5355-2020>
- Zhang, Q., Jiang, X., Tong, D., Davis, S. J., Zhao, H., Geng, G., et al. (2017b). Transboundary health impacts of transported global air pollution and international trade. *Nature*, 543(7647), 705–709. <https://doi.org/10.1038/nature21712>
- Zhang, Y., Schauer, J. J., Zhang, Y., Zeng, L., Wei, Y., Liu, Y., & Shao, M. (2008). Characteristics of particulate carbon emissions from real-world Chinese coal combustion. *Environmental Science & Technology*, 42(14), 5068–5073. <https://doi.org/10.1021/es7022576>
- Zhang, Y., Yuan, Q., Huang, D., Kong, S., Zhang, J., Wang, X., et al. (2018a). Direct observations of fine primary particles from residential coal burning: Insights into their morphology, composition, and hygroscopicity. *Journal of Geophysical Research: Atmospheres*, 123(22), 12964–12979. <https://doi.org/10.1029/2018JD028988>
- Zhang, Y.-L., El-Haddad, I., Huang, R.-J., Ho, K.-F., Cao, J.-J., Han, Y., et al. (2018b). Large contribution of fossil fuel derived secondary organic carbon to water soluble organic aerosols in winter haze in China. *Atmospheric Chemistry and Physics*, 18(6), 4005–4017. <https://doi.org/10.5194/acp-18-4005-2018>
- Zhao, C., & Garrett, T. J. (2015). Effects of Arctic haze on surface cloud radiative forcing. *Geophysical Research Letters*, 42(2), 557–564. <https://doi.org/10.1002/2014gl062015>
- Zhao, J., Qiu, Y., Zhou, W., Xu, W., Wang, J., Zhang, Y., et al. (2019). Organic aerosol processing during winter severe haze episodes in Beijing. *Journal of Geophysical Research: Atmospheres*, 124(17–18), 10248–10263. <https://doi.org/10.1029/2019jd030832>
- Zhao, X. J., Zhao, P. S., Xu, J., Meng, W., Pu, W. W., Dong, F., et al. (2013). Analysis of a winter regional haze event and its formation mechanism in the North China Plain. *Atmospheric Chemistry and Physics*, 13(11), 5685–5696. <https://doi.org/10.5194/acp-13-5685-2013>
- Zheng, G. J., Duan, F. K., Su, H., Ma, Y. L., Cheng, Y., Zheng, B., et al. (2015). Exploring the severe winter haze in Beijing: The impact of synoptic weather, regional transport and heterogeneous reactions. *Atmospheric Chemistry and Physics*, 15(6), 2969–2983. <https://doi.org/10.5194/acp-15-2969-2015>
- Zheng, H., Kong, S., Wu, F., Cheng, Y., Niu, Z., Zheng, S., et al. (2019). Intra-regional transport of black carbon between the south edge of the North China Plain and central China during winter haze episodes. *Atmospheric Chemistry and Physics*, 19(7), 4499–4516. <https://doi.org/10.5194/acp-19-4499-2019>
- Zhong, J., Zhang, X., Wang, Y., Wang, J., Shen, X., Zhang, H., et al. (2019). The two-way feedback mechanism between unfavorable meteorological conditions and cumulative aerosol pollution in various haze regions of China. *Atmospheric Chemistry and Physics*, 19(5), 3287–3306. <https://doi.org/10.5194/acp-19-3287-2019>
- Zhu, Y., Li, W., Lin, Q., Yuan, Q., Liu, L., Zhang, J., et al. (2020). Iron solubility in fine particles associated with secondary acidic aerosols in east China. *Environmental Pollution*, 264, 114769. <https://doi.org/10.1016/j.envpol.2020.114769>